
Ames Research Center Shear Tests of SLA-561V Heat Shield Material for Mars-Pathfinder

Huy Tran, Michael Tauber, William Henline,
Duoc Tran, Alan Cartledge, Frank Hui, and
Norm Zimmerman

September 1996



National Aeronautics and
Space Administration

Ames Research Center Shear Tests of SLA-561V Heat Shield Material for Mars-Pathfinder

Huy Tran, Ames Research Center, Moffett Field, California

Michael Tauber, Duoc Tran, and Norm Zimmerman, Thermosciences Institute,
Moffett Field, California

William Henline, Alan Cartledge, and Frank Hui, Ames Research Center,
Moffett Field, California

September 1996



National Aeronautics and
Space Administration

Ames Research Center
Moffett Field, California 94035-1000

TABLE OF CONTENTS

	Page
Summary	1
Introduction	1
Background on Mars-Pathfinder	1
Agreements Between Ames Research Center and Jet Propulsion Laboratory	1
Objectives of Current Test Series	1
Test Conditions	2
Analytical Predictions of the Entry Environment	2
Derived Conditions for Arc-Jet Tests	2
Model Assembly, Instrumentation, and Facility Description	3
Material Description	3
Test Model Design	3
Test Facility Description	4
Calibration Procedure	4
Results	4
Ablation Models	7
Repaired Models	7
In-depth Temperature Response	9
Concluding Remarks	10
Appendix A	11

List of Tables

		Page
1	Calculated conditions for a “steep” (severe) entry	2
2	Shear and heating test conditions for shear models	3
3	Test conditions	5
4	Ablation test model performance	6
A-1	Thermocouple data and model cross reference	13

List of Figures

		Page
1	Non-ablating shear stress distribution over Mars-Pathfinder forebody	2
2	Comparisons of flight and test peak shear stresses	3
3	Pathfinder heating rate distribution	3
4	2" × 9" arc-heated Turbulent Duct Facility test section	4
5	(a) Average recession vs. integrated shear load, (b) total mass loss vs. integrated shear load	7
6	(a) Average recession vs. integrated heat load, (b) total mass loss vs. integrated heat load.....	8
7	Surface inflation measurements around repairs on model SLAP08R.....	8
8	Surface inflation measurements around repairs on model SLAP09R.....	8
9	Surface recession measurements around repairs on model SLAP11R	9
10	(a),(b) In-depth temperature response to 31 sec exposure, from model SLAP05TC-3,	9
11	(a),(b) In-depth temperature response to 48 sec exposure, from model SLAP07TC-3,	10
A.1	Schematic of models SLAP01, SLAP02, SLAP03, and SLAP04	14
A.2	Schematic of model SLAP05	15
A.3	Schematic of model SLAP06	16
A.4	Schematic of model SLAP07	17
A.5	Schematic of model SLAP08	18
A.6	Schematic of model SLAP09	19
A.7	Schematic of model SLAP10	20
A.8	Schematic of model SLAP11	21
A.9	Pre- and post-test photos of model SLAP01-1 (a) Ablation model SLAP01-1, (b) SLAP01-1 after 76 sec @ $\tau = 170 \text{ N/m}^2$, $\dot{q} = 21.6 \text{ W/cm}^2$	22
A-10	Pre- and post-test photos of model SLAP02-2. (a) Ablation model SLAP02-2, (b) SLAP02-2 after 39 sec @ $\tau = 240 \text{ N/m}^2$, $\dot{q} = 40 \text{ W/cm}^2$	23
A-11	Pre- and post-test photos of model SLAP03-3. (a) Ablation model SLAP03-3, (b) SLAP03-3 after 37 sec @ $\tau = 390 \text{ N/m}^2$, $\dot{q} = 51 \text{ W/cm}^2$	24
A-12	Pre- and post-test photos of model SLAP04-3. (a) Ablation model SLAP04-3, (b) SLAP04-3 after 41 sec @ $\tau = 390 \text{ N/m}^2$, $\dot{q} = 51 \text{ W/cm}^2$	24
A-13	Pre- and post-test photos of model SLAP05TC-3. (a) Instrumented model SLAP05TC-3, (b) SLAP05TC-3 after 31 sec @ $\tau = 390 \text{ N/m}^2$, $\dot{q} = 51 \text{ W/cm}^2$	26
A-14	Pre- and post-test photos of model SLAP06TC-2. (a) Instrumented model SLAP06TC-2, (b) SLAP06TC-2 after 38 sec @ $\tau = 240 \text{ N/m}^2$, $\dot{q} = 40 \text{ W/cm}^2$	27
A-15	Pre- and post-test photos of model SLAP07TC-3. (a) Instrumented model SLAP07TC-3,	

	(b) SLAP07TC-3 after 48 sec @ $\tau = 390 \text{ N/m}^2$, $\dot{q} = 51 \text{ W/cm}^2$	28
A-16	Pre- and post-test photos of model SLAP08R-3. (a) Repair plug and gap model SLAP08R-3, (b) SLAP08R-3 after 38 sec @ $\tau = 390 \text{ N/m}^2$, $\dot{q} = 51 \text{ W/cm}^2$	29
A-17	Pre- and post-test photos of model SLAP09R-3. (a) Repair plug and gap model SLAP09R-3, (b) SLAP09R-3 after 40 sec @ $\tau = 390 \text{ N/m}^2$, $\dot{q} = 51 \text{ W/cm}^2$	30
A-18	Pre- and post-test photos of model SLAP10R-3. (a) Gap model SLAP10R-3, (b) SLAP10R-3 after 38 sec @ $\tau = 390 \text{ N/m}^2$, $\dot{q} = 51 \text{ W/cm}^2$	31
A-19	Pre- and post-test photos of model SLAP11R-3. (a) Repair plug model SLAP11R-3, (b) SLAP11R-3 after 36 sec @ $\tau = 390 \text{ N/m}^2$, $\dot{q} = 51 \text{ W/cm}^2$	32
A-20	Recession contour plots of model SLAP01-1	33
A-21	Recession contour plots of model SLAP02-2	34
A-22	Recession contour plots of model SLAP03-3	35
A-23	Recession contour plots of model SLAP04-3	36
A-24	Recession contour plots of model SLAP05TC-3	37
A-25	Recession contour plots of model SLAP06TC-2	38
A-26	Recession contour plots of model SLAP07TC-3	39
A-27	Recession contour plots of model SLAP08R-3	40
A-28	Recession contour plots of model SLAP09R-3	41
A-29	Recession contour plots of model SLAP10R-3	42
A-30	Recession contour plots of model SLAP11R-3	43

Ames Research Center Shear Tests of SLA-561V Heat Shield Material for Mars-Pathfinder

HUY TRAN, MICHAEL TAUBER,*† WILLIAM HENLINE, DUOC TRAN,* ALAN CARTLEDGE, FRANK HUI, AND NORM ZIMMERMAN*

Ames Research Center

Summary

This report describes the results of arc-jet testing at Ames Research Center on behalf of Jet Propulsion Laboratory (JPL) for the development of the Mars-Pathfinder heat shield. The current test series evaluated the performance of the ablating SLA-561V heat shield material under shear conditions. In addition, the effectiveness of several methods of repairing damage to the heat shield were evaluated. A total of 26 tests were performed in March 1994 in the 2" × 9" arc-heated Turbulent Duct Facility, including runs to calibrate the facility to obtain the desired shear stress conditions. A total of eleven models were tested. Three different conditions of shear and heating were used. The non-ablating surface shear stresses and the corresponding, approximate, non-ablating surface heating rates were as follows: Condition I, 170 N/m² and 22 W/cm²; Condition II, 240 N/m² and 40 W/cm²; Condition III, 390 N/m² and 51 W/cm². The peak shear stress encountered in flight is represented approximately by Condition I; however, the heating rate was much less than the peak flight value. The peak heating rate that was available in the facility (at Condition III) was about 30 percent less than the maximum value encountered during flight. Seven standard ablation models were tested, of which three models were instrumented with thermocouples to obtain in-depth temperature profiles and temperature contours. An additional four models contained a variety of repair plugs, gaps, and seams. These models were used to evaluate different repair materials and techniques, and the effect of gaps and construction seams. Mass loss and surface recession measurements were made on all models. The models were visually inspected and photographed before and after each test. The SLA-561V performed well; even at test Condition III, the char remained intact. Most of the resins used for repairs and gap fillers performed poorly. However, repair plugs made of SLA-561V performed well. Approximately 70 percent of the thermocouples yielded good data.

Introduction

Background on Mars-Pathfinder

The Mars-Pathfinder project will develop and verify technology for future scientific probe missions to Mars. This technology development includes demonstrating direct ballistic entry into the Martian atmosphere from an interplanetary trajectory, aerodynamic deceleration, and soft-landing in a preferred attitude.

Agreements Between Ames Research Center and Jet Propulsion Laboratory

The Jet Propulsion Laboratory (JPL) has requested support from Ames Research Center (ARC) in the analysis, design and testing of the vehicle's heat shield material. The heat shield subsystem protects the lander from the heat of atmospheric entry and decelerates the vehicle to speeds at which the parachute can be deployed safely. A variety of tests and analyses have been performed at ARC to develop the entry heat shield subsystem. These tests have included the following: screening tests of candidate ablation materials; testing of the SLA-561V ablator to much higher heat fluxes than experienced by Viking; and defining the pressure limit of SLA-561V to be 0.25 atm. In addition, the impact of cold-soak exposure on the ablator was evaluated. Many of the procedures used in the current test series are similar to those of the previously performed tests.

Objectives of Current Test Series

- Assess the thermo-mechanical integrity of SLA-561V under high shear conditions, at heating rates that approach the flight heating rates as closely as possible.
- Assess the effects of repair procedures and gap filler materials on heat shield integrity.

*Thermosciences Institute, Moffett Field, California.

†Project Lead.

Test Conditions

During entry, the heat shield must withstand a combination of thermal and mechanical loads. Previous tests performed in the ARC 60 MW Interactive Heating Facility (see "Ames Research Center arc-jet Facility Tests of Candidate Heat Shield Materials for MESUR-Pathfinder," Feb. 1994) indicated that the recession rate of SLA-561V varies directly with the applied stagnation pressure and heating rate. However, due to the test model configuration, the shear stresses produced on corners of the 60 MW test models were several times the levels expected during flight, making it difficult to realistically assess the material's performance in its intended environment. The current test series was designed to evaluate the material's performance under more representative shear conditions by using a flat panel model in a parallel flow type of facility.

Analytical Predictions of the Entry Environment

The peak shear stresses on the aeroshell during entry are shown in figure 1; the steepest trajectory under consideration at the present time (-16.2 deg) was assumed. The abscissa, S, is the arc length along the surface from the stagnation point.

The shear stresses were calculated using the GIANTS code, which solves the Navier-Stokes equations over the forebody, neglecting the effects of ablation. Ablation will reduce the surface shear stress below the values shown in figure 1. The assumptions used in the calculations, and the results pertinent to this test series, are shown in table 1. The trajectory parameters were arrived at jointly by ARC and JPL in February 1994.

Derived Conditions for Arc-Jet Tests

The test program examined the behavior of SLA-561V heat shield material at the peak shear stress predicted for

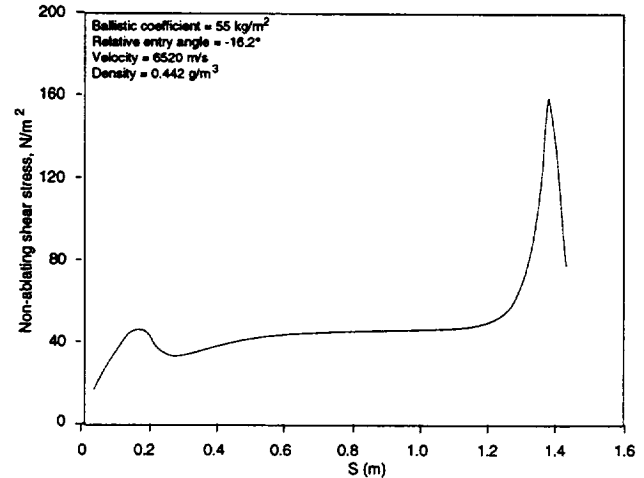


Figure 1. Non-ablating shear stress distribution over Mars-Pathfinder forebody.

the trajectory described above. Three shear levels were chosen for this test series, as summarized in table 2. Condition I represents a value about 10 percent higher than the maximum shear stress predicted for the flight case shown in figure 1. Test Condition II represents an intermediate level between Conditions I and III. Test Condition III reproduces the shear condition encountered during previous tests in arc 60 MW IHF. The IHF tests produced heating rates and stagnation pressures appropriate for the vehicle's stagnation point (approximately 100 W/cm² and 0.22 atm). However, the stagnation point models produced unrealistically high shear stresses on the model corners, and correspondingly high rates of erosion. Test Condition III of the current series was chosen to check the ablator's performance for consistency with the previous test results. In addition, Condition III comes closest to reproducing the peak flight heating rate at the body location where the maximum shear stress occurs.

Table 1. Calculated conditions for a "steep" (severe) entry

Trajectory simulation input parameters	
Ballistic coefficient (m/C _d A)	55 kg/m ²
Entry velocity (at 125 km altitude)	7.65 km/s
Entry angle (at 125 km altitude)	-16.2°
Simulation Results (non-ablating surface) V = 6521 m/s, r = 0.442 g/m ³	
Peak shear stress	158 N/m ²
Heating rate at peak shear location	75 W/cm ²

Table 2. Shear and heating test conditions for shear models

Condition no.	Description	Shear stress, N/m ²	Heating rate, W/cm ²
I	Maximum predicted shear stress for flight with $\beta = 55 \text{ kg/m}^2$, $\gamma = -16.2^\circ$	170	22
II	Intermediate shear level	240	40
III	Shear stress of 60 MW IHF test series at stagnation pressure of 0.221 atm.	390	51

The shear stresses shown in table 2 were the most significant test parameter; the heating rates are the product of the corresponding arc-jet settings. The shear and heating rate values shown represent peak test conditions, and do not include the variations associated with starting and shutting down the test facility. While it is impossible to match both the peak shear and heating rate in the facility to the flight levels, the total heat load was approximately matched by varying the test duration. The exposure times were selected to match the total (non-ablating) heat load at the body location of maximum shear stress. Figure 2 compares the non-ablating shear stresses used during this test program with those predicted for the Mars-Pathfinder trajectory, and those of the earlier 60 MW IHF tests. Figure 3 shows the non-ablating surface heating rates for the same flight trajectory.

Model Assembly, Instrumentation, and Facility Description

Material Description

SLA-561V is a low density ablator produced by the Michoud Division of Lockheed-Martin. The material consists of ground cork, phenolic micro-balloons, reinforcing glass fibers, eccospheres, and elastomeric silicone, in a phenolic honeycomb support structure. The honeycomb used for SLA-561V is Hexcel Corporation's F35, with a cell size of 0.86 cm.

Test Model Design

The 20.3 cm × 50.8 cm × 6.35 cm model assembly used in this test series consisted of a rectangular brick of ablative material, 15.2 cm wide by 25.4 cm long by 2.54 cm thick, bonded to a 0.64 cm thick aluminum backplate. The ablator was insulated from the water-cooled test chamber walls by a frame of Toughened Uni-piece Fibrous insulation (TUFI), and was secured to a aluminum baseplate

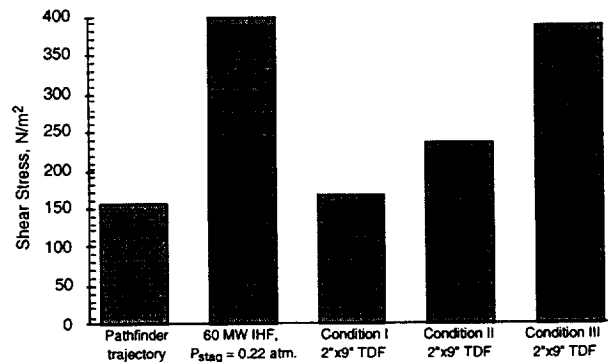


Figure 2. Comparisons of flight and test peak shear stresses.

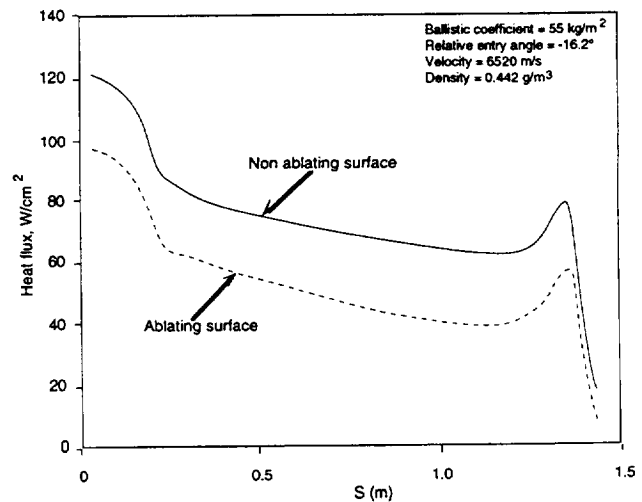


Figure 3. Pathfinder heating rate distribution.

by four 1/4"-20 screws. Seven ablation models were tested, of which three were instrumented with thermocouples. In addition, four models were used to evaluate different repair plugs, gap fillers, or standard seams. One of

the seven ablation models was cut in half. The first half was instrumented with thermocouples and the other was retained for future use. The thermocouples on all three instrumented models were installed near the surface (at 0.25 cm depth), at various depths within the ablator, and on the adhesive bondline between the ablator and the aluminum backplate. The figures in Appendix A show the locations of the installed thermocouples for each model. arc personnel instrumented all of the models used in this test series.

Test Facility Description

The 2" x 9" arc-heated Turbulent Flow Duct Facility is a supersonic blow-down type wind tunnel using an electric arc heater and capable of continuous operation within power supply limit. Presently in use is a Linde type arc heater that can produce stream enthalpies up to 5.8 MJ/kg (2500 BTU/lb) and maximum free stream Mach number of 3.5. The test gas (air in this case) is heated by an electrical discharge and the supersonic flow is then expanded into a test chamber through a two-dimensional nozzle exit. The test chamber, shown schematically in figure 4, is a water-cooled rectangular structure made of copper side and end plates bolted together to form a 5 cm x 23 cm (2" x 9") test section. The test panel is mounted flush on the test section's widest side, and the wall opposite the test section is instrumented with pressure ports and flush-mounted calorimeters. Unlike the 60 MW IHF, where the model is mounted on a moveable sting, the test model is exposed to the flow from start up until the facility is shut down. This fact is important because the starting transient can be a large fraction of the model's exposure time to the stream.

Calibration Procedure

Since it was not possible to directly measure the shear stress generated on the model, a series of calibration runs were performed on a special calibration model to obtain

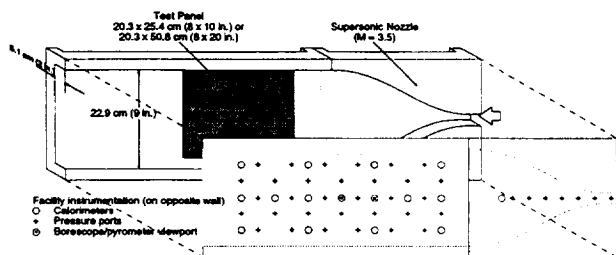


Figure 4. 2" x 9" arc-heated Turbulent Duct Facility test section.

the necessary parameters for the shear stress calculation. The calibration model, made of a re-usable tile material with a TUF1 coating, is 20.3 cm wide by 25.4 cm long by 5.08 cm thick. In the calibration runs, the six surface thermocouples were used to verify the arc heater settings (current, voltage, manifold pressure, and chamber pressure) that were required to produce the appropriate shear stress over the model. The heat flux gages and pressure sensors mounted on the opposite wall were used to check the repeatability of the test conditions.

The shear stress on the model was calculated by using Reynold's analogy for a fully turbulent flow and assuming that the Prandtl number is approximately unity. The surface temperatures extracted from the calibration runs were employed in the hot wall heating rate calculation using the Stefan-Boltzmann equation for radiative equilibrium, neglecting conduction into the depth of the material. The total enthalpy of the stream was estimated from the facility's power input and assuming a heater efficiency of 50 percent. The shear stress is then calculated from the hot wall heating rate and flow total enthalpy.

Since the model is exposed to the flow from the time of start-up, a special effort was made to ensure that all models experience about the same start up conditions and exposure times. Eight calibration test runs were conducted, several at each condition, to obtain statistical data on the heating rate and stagnation pressure, and to check the repeatability of the facility. Several calibration test runs without calibration models were also made to obtain the cold wall heating rates. In these runs, a water cooled blank-off plate was used such that both walls of the test chamber were cooled. The runs which produced the desired shear conditions gave the set points that were used for the remaining tests.

Results

Table 3 summarizes the test conditions and table 4 contains the ablation performance of the models tested. The mass losses and surface recessions were determined from the pre- and post-test measurements of total weight and changes in the thickness of each sample. Each sample's thickness was measured before and after the test, using a template to ensure the measurements were made at the same points. This measurement technique allows the surface recession contours to be plotted. The integrated shear load parameter used here is defined as the approximate, non-ablating, shear stress multiplied by the time at the desired test condition. The total heat load was estimated by multiplying the non-ablating heating rate (shown in table 3) by the time at test condition. For both of these parameters, the heating rate and shear stress at start up are

Table 3. Test conditions

Model ID	Date	Shear stress, N/m ²	Heat flux, W/cm ²	Arc-jet current, amps	Chamber pressure, kPa	Exposure time, sec	Pyro temp., $\epsilon = 1$, °C	Model type
SLAP01-1	3/8/94	170	21.6	2000	362	76	1117	Ablation
SLAP02-2	3/8/94	240	40	2500	512	39	1252	Ablation
SLAP03-3	3/9/94	390	51	2700	894	37	1349	Ablation
SLAP04-3	3/9/94	390	51	2700	923	41	1409	Ablation
SLAP05TC-3 (half model)	3/23/94	390	51	2700	889	31	1416	12 Thermocouples
SLAP06TC-2	3/10/94	240	40	2500	518	38	1314	13 Thermocouples
SLAP07TC-3	3/28/94	390	51	2700	909	48	1403	20 Thermocouples
SLAP08R-3	3/14/94	390	51	2700	917	38	1405	2 Repair plugs, and a 0.076 cm filled gap perpendicular to flow
SLAP09R-3	3/15/94	390	51	2700	944	40	1373	4 Repair plugs and a standard bondline gap
SLAP10R-3	3/14/94	390	51	2700	930	38	1411	2 Gaps parallel to flow; one 0.076 cm wide and one standard bondline
SLAP11R-3	3/28/94	390	51	2700	930	36	1413	4 Repair plugs

Table 4. Ablation test model performance

Model ID	Integrated shear load, N-sec/m ²	Initial mass, grams	Final mass, grams	Mass loss, grams	Average initial thick., cm	Average final thick., cm	Average recession, cm
SLAP01-1	12,900	1232.6	1203.5	29.1	3.488	3.453	0.034
SLAP02-2	9360	1226.9	1199.3	27.6	3.484	3.444	0.040
SLAP03-3	14,400	1227.4	1199.3	28.1	3.488	3.434	0.054
SLAP04-3	16,000	1231.2	1200.4	30.8	3.485	3.423	0.062
SLAP05TC-3	12,100	623.6	609.1	14.5	3.490	3.438	0.052
SLAP06TC-3	9120	1248.0	1219.5	28.5	3.485	3.443	0.041
SLAP07TC-3	18,700	1248.5	1218.3	30.2	3.488	3.423	0.065
SLAP08R-3	14,800	1266.3	1235.0	31.3	3.484	3.442	0.043
SLAP09R-3	15,600	1249.9	1219.3	30.6	3.481	3.436	0.046
SLAP10R-3	14,800	1245.8	1215.9	29.9	3.487	3.437	0.050
SLAP11R-3	14,000	1248.4	1215.0	33.4	3.488	3.437	0.051

fairly small and were therefore ignored in calculating the integrated heating and shear load. Each model's surface temperatures were measured during the test with a Mikron pyrometer operating at infra-red wavelengths (800 nanometers) through a view-port on the opposite wall. An emissivity of unity was assumed in converting the pyrometer readings to the peak temperatures listed in table 3.

Figures 5(a) and (b) show the average recession and total mass loss as a function of the integrated shear load. Although the scatter in the data approached ± 15 percent, the recession trend is a fairly smooth function of the integrated shear load. The low average surface recession of model #1 is likely the result of the low heating rate; however, the temperatures were high enough to cause the resin to pyrolyze sufficiently to produce a mass loss comparable to that of the other models. No anomalous mass removal is evident from figure 5(b). Note that the mass loss measurements from the three models with repair plugs (#8, #9, and #11) were deliberately excluded from figure 5(b), to avoid mixing mass loss from the repair materials with that from the heat shield material.

Ablation Models

Four models, without repairs or gaps, were tested to evaluate the ablation characteristics of SLA-561V at three shear conditions. The material performed well at all three conditions; even at Condition III, there was no visible char damage. There was a variation of a few grams in total mass loss from Condition I to Condition III. Otherwise there was no significant difference in the performance of the material, despite small variations in the time at test conditions. The independent parameter in this case was the integrated shear load, defined as the non-ablating

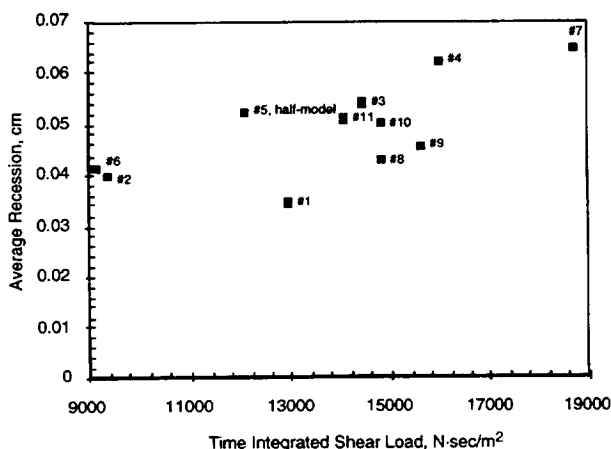
hear stress multiplied by the time at test conditions. Figure 6(a) shows the total variation of mass loss with the integrated shear load, and figure 6(b) shows the total mass loss as a function of heat load. The results shown in figures 6(a) and (b) are very similar to those illustrated and discussed previously in figures 5(a) and (b). As explained above for figure 5(b), the data from the repair models were excluded from the mass loss data shown in figure 6(b). Visual inspection of the models' surfaces showed well-adhered char layers. No excessive surface erosion, spallation or uneven melting were detected. On the models tested at Condition III, small droplets condensed on the phenolic honeycomb structure, indicating that some melting had occurred.

However, there were significant differences in surface recession at each test condition. The sample tested at Condition I had an average recession of about 0.034 cm, about 0.041 cm for samples tested at Condition II, and about 0.054 cm for Condition III. A common feature observed in samples from all three conditions was the comparatively higher recession near the outer edges than in the center. This is illustrated in the recession contour plots for each model in Appendix A. Note that sample SLAP04-3 had a slightly higher recession at the edges than the other samples tested at the same Condition III, because some flow penetrated into a narrow gap between the model and frame.

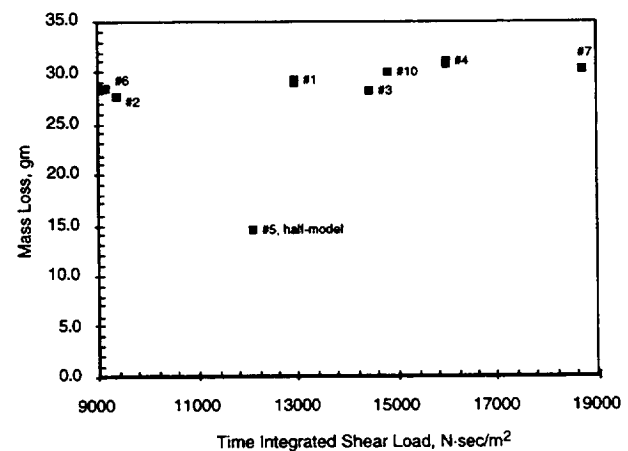
Repaired Models

Model illustrations and labels are given in Appendix A.

SLAP08R-3— This model, illustrated on page 18 of Appendix A, had four repair plugs, each covering



(a)



(b)

Figure 5. (a) Average recession vs. integrated shear load, (b) total mass loss vs. integrated shear load.

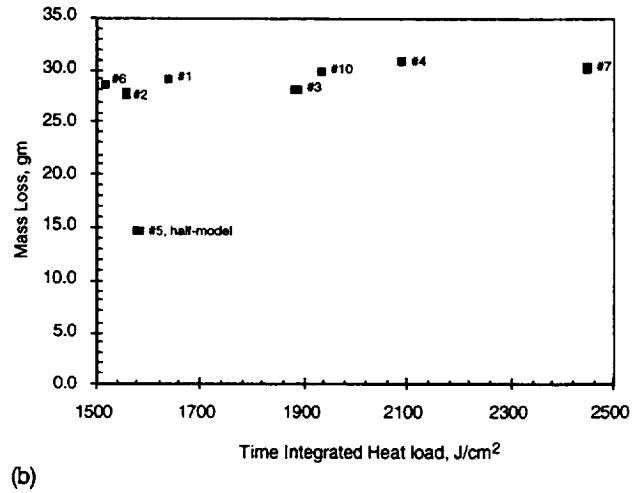
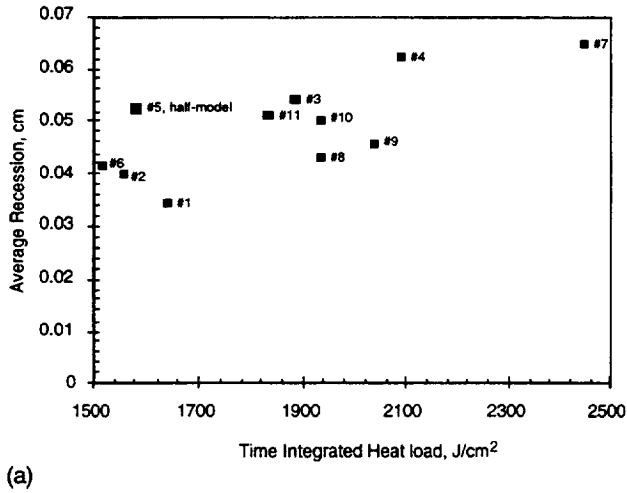


Figure 6. (a) Average recession vs. integrated heat load, (b) total mass loss vs. integrated heat load.

approximately 9 cells (3 × 3 cells). A filled gap, 0.076 cm wide, ran completely across the model perpendicular to the flow. All four plugs experienced cracking; this was most extensive on plugs #2 and #3. A significant amount of material was removed by spallation and vaporization, and large cracks appeared on these two repair plugs. The surfaces of all plugs inflated (rose above the surrounding surface) to an average of about 0.13 cm; the inflation is plotted in figure 7. The gap filler material melted, forming a forward-facing step to the flow. This step increased the local heating and material erosion near the center of the model.

SLAP09R– This model, illustrated on page 19 of Appendix A, had four repair plugs, each covering

approximately 4 cells (2 × 2 cells). It also had a gap, described by Lockheed-Martin-Michoud as a “standard bondline” gap, running perpendicular to the flow. This gap, nominally 0.013 cm wide, performed very well; no significant enlargement, melting, or erosion was observed. As in the SLAP08R model, all four repair plugs experienced cracking and inflation. However, as figure 8 shows, repair plugs #1 and #3 (the upstream plugs) experienced more inflation than plugs #2 and #4 (the downstream plugs).

SLAP10R– This model, illustrated on page 20 of Appendix A, had two gaps running the length of the model, parallel to the flow direction. One was a standard bondline gap and the other was a 0.076 cm wide gap filled

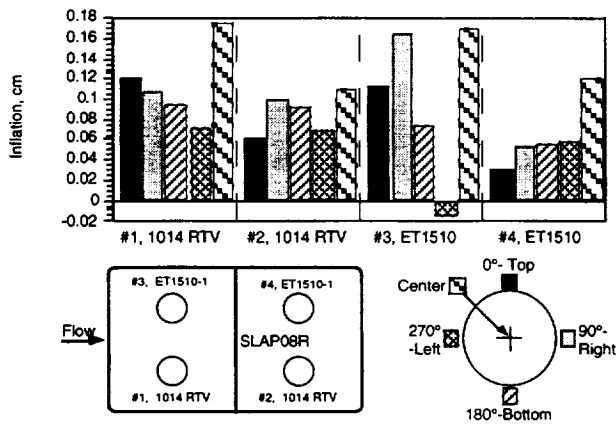


Figure 7. Surface inflation measurements around repairs on model SLAP08R.

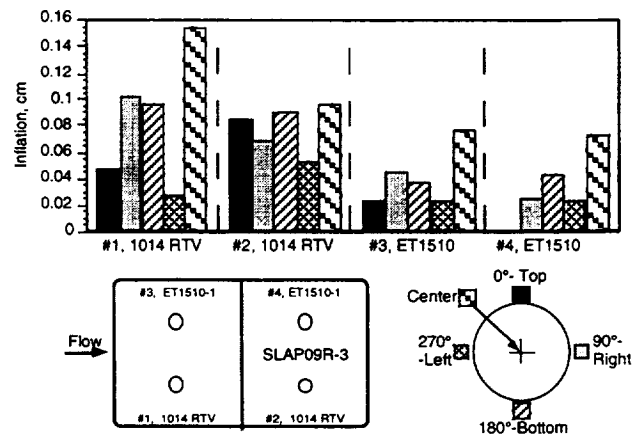


Figure 8. Surface inflation measurements around repairs on model SLAP09R.

with GX-6300 resin. As in the prior test, the standard bondline was essentially unaffected by the hot gas. The 0.076 cm gap was widened by flow penetration and melt run-off was observed near the gap surface. Unlike the SLAP08R model, surface erosion or material depletion was not increased.

SLAP11R– This model, illustrated on page 21 of Appendix A, had four repair plugs. The two upstream repairs covered approximately 9 cells (3 × 3) and the other two covered approximately 4 cells (2 × 2). The repair plugs #1 and #2, shown on the left in the figure, were made of SLA-561V, including the honeycomb reinforcement, bonded with GX-6300. These plugs performed well, recessing 0.05 cm, and no cracking was observed. The downstream repair (plug #2) did not perform as well as the upstream repair plug, however, because the inserted core fit poorly into the opening. Repair plugs #3 and #4, shown on the right in the figure, had honeycomb cores hand-packed with ET1510-I resin. These repair plugs experienced some cracking and inflation. Cell size did not seem to have a significant impact on the repair performance. Figure 9 shows that repair plugs filled with ET1510-I inflated about 0.038 cm.

In-depth Temperature Response

Three models were instrumented with a total of 45 thermocouples at various locations and depths to obtain temperature contours and thermal response histories. One model was tested at Condition II, the other two were tested at Condition III, with different test durations. Due to limitations of the facility instrumentation, some of the

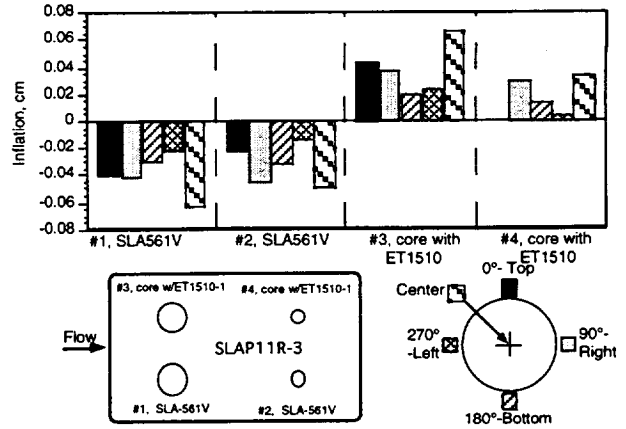
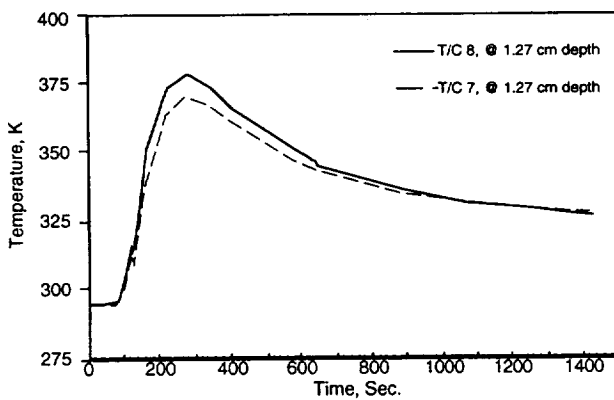
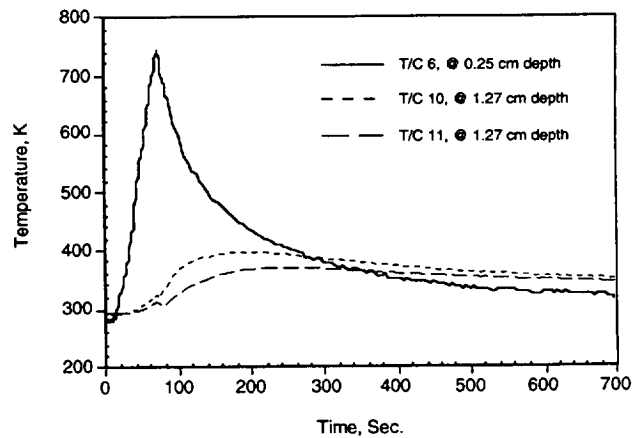


Figure 9. Surface recession measurements around repairs on model SLAP11R.

thermocouples were connected to a strip chart recorder. Thirty-one thermocouples, or about 70 percent, produced usable data. The figures in Appendix A (pages 15–17) show the location and depth of each model’s thermocouples. Figures 10(a) and (b) show the in-depth temperature response after 31 sec of exposures to Condition III, while figures 11(a) and (b) show a typical response after 48 sec of exposure. The temperatures indicated in figures 10(a) and (b) are smooth, while those in figures 11(a) and (b) show some noise. The 5 to 7 percent variation in the peak temperatures recorded by the gages installed 0.25 cm below the surface probably reflects primarily the variation of heating rate over the model.

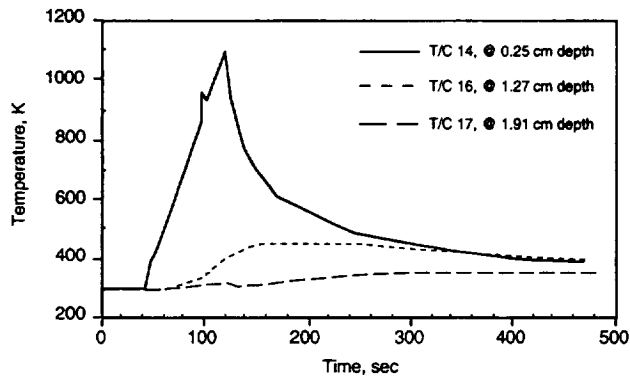


(a)

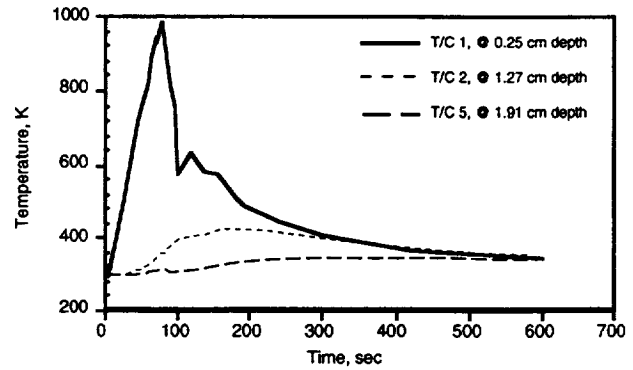


(b)

Figure 10. (a) In-depth temperature response to 31 sec exposure, from model SLAP05TC-3, (b) in-depth temperature response to 31 sec exposure, from model SLAP05TC-3.



(a)



(b)

Figure 11. (a) In-depth temperature response to 48 sec exposure, from model SLAP07TC-3, (b) in-depth temperature response to 48 sec exposure, from model SLAP07TC-3.

Concluding Remarks

A total of eleven flat panel models of SLA-561V ablative material were tested in the arc-heated Turbulent Duct Facility. Three of the models were instrumented with thermocouples and four others contained a variety of repair plugs, gaps, and seams. The objective of the current test was to expose the ablating SLA-561V to more realistic shear stresses acting over a larger area than had been possible during the previous arc-jet facility tests performed at ARC during the November 1993 through January 1994 time period. The non-ablating surface shear stresses in the current test series ranged from being about 8 to 250 percent higher than the peak flight value, but the corresponding test heating rates were only about 30 to 70 percent, respectively, of the maximum flight rates, due to facility limitations. However, the peak flight values of shear and the accompanying heating rate occur only over a very small fraction of the forebody's surface, near the rim or outer skirt region of the vehicle.

The over-all conclusion from the present test series is that the SLA-561V ablator exhibited no excessive char

removal or spallation. Even at the most severe shear test condition, which exceeded the flight shear level by 250 percent, the char remained intact, thus preserving its ability to re-radiate heat. Although the test heating rates were less than the peak flight rates, the SLA-561V should withstand the shear stresses that are expected during entry.

The only heat shield repair method that was effective in the tests was to embed the resin in a phenolic honeycomb core plug to protect the filler from excessive erosion. The standard bondline gaps of 0.013 cm width withstood the test environment well. In contrast, the filler used on the wider, 0.076 cm gaps, melted or vaporized to a significant depth, and caused the seams to widen.

Of the total of 45 thermocouples embedded in three models, 31 yielded usable data. Hopefully, this 70 percent success rate can be improved in future tests. However, the ability to obtain reliable thermocouple data in arc-jet facilities remains a potential problem.

APPENDIX A

Appendix A

Thermocouple cross-reference table, model figures, model pre- and post-test photos, and recession contour plots.

The following table lists the thermocouples in the three instrumented models which produced valid data, available for further analysis. Those thermocouples not listed here produced invalid or suspect data, due to ground loops, shorts, inadequate shielding, or other instrumentation problems. The depth of the thermocouple from the surface is given; the model illustrations on the following pages detail each thermocouple's location within the model.

Table A-1. Thermocouple data and model cross reference

Model ID T/C no.	Depth, cm	Model ID T/C no.	Depth, cm	Model ID T/C no.	Depth, cm
SLAP05-1	0.25	SLAP06-2	0.25	SLAP07-2	0.25
SLAP05-2	0.25	SLAP06-5	0.25	SLAP07-3	0.25
SLAP05-3	0.25	SLAP06-6	0.25	SLAP07-5	0.25
SLAP05-4	0.25	SLAP06-10	0.25	SLAP07-6	0.25
SLAP05-5	0.25			SLAP07-7	1.27
SLAP05-6	0.25			SLAP07-9	2.54
SLAP05-7	1.27			SLAP07-10	0.25
SLAP05-9	2.54			SLAP07-11	1.27
SLAP05-10	1.27			SLAP07-12	1.91
SLAP05-11	1.27			SLAP07-13	2.54
SLAP05-12	2.54			SLAP07-14	0.25
				SLAP07-15	2.54
				SLAP07-16	1.91
				SLAP07-17	1.27
				SLAP07-19	1.91
				SLAP07-20	2.54

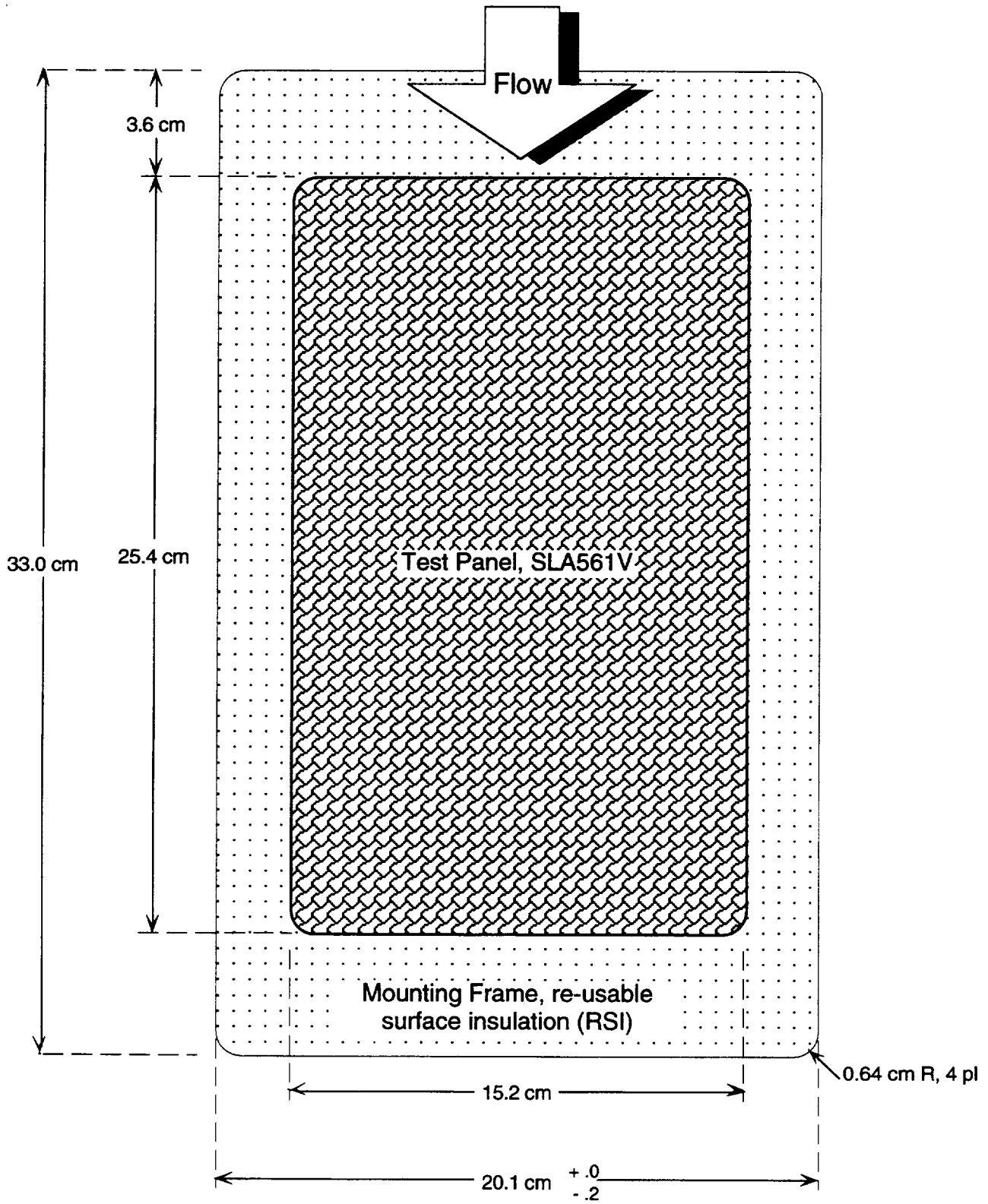
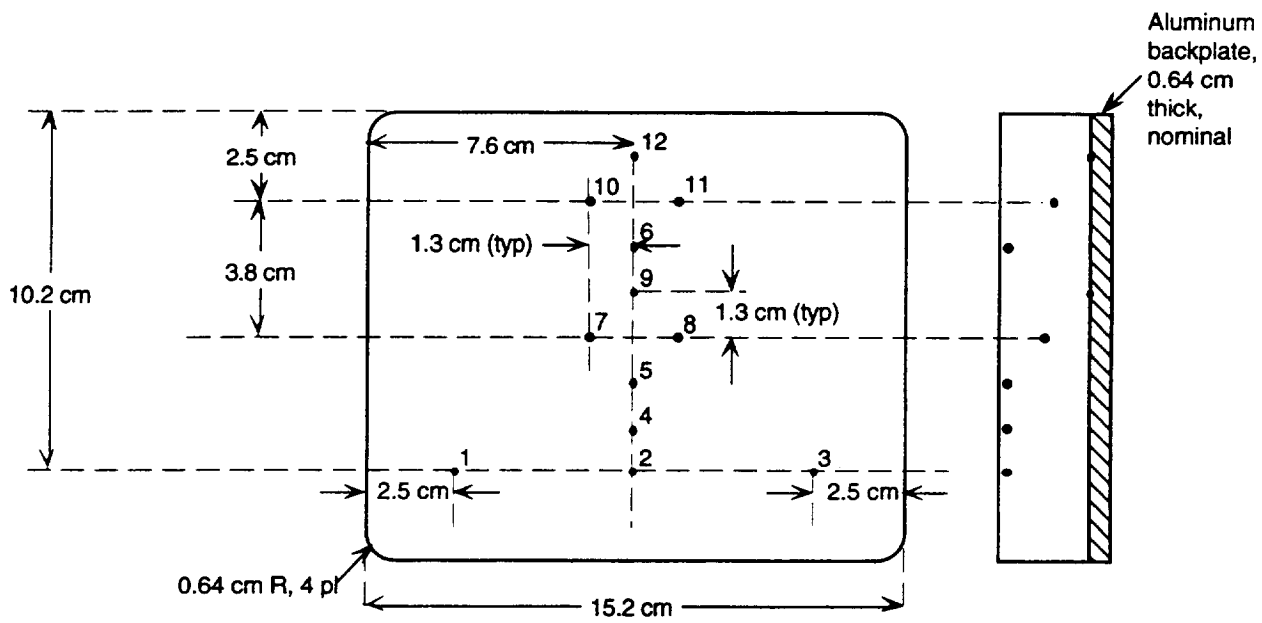


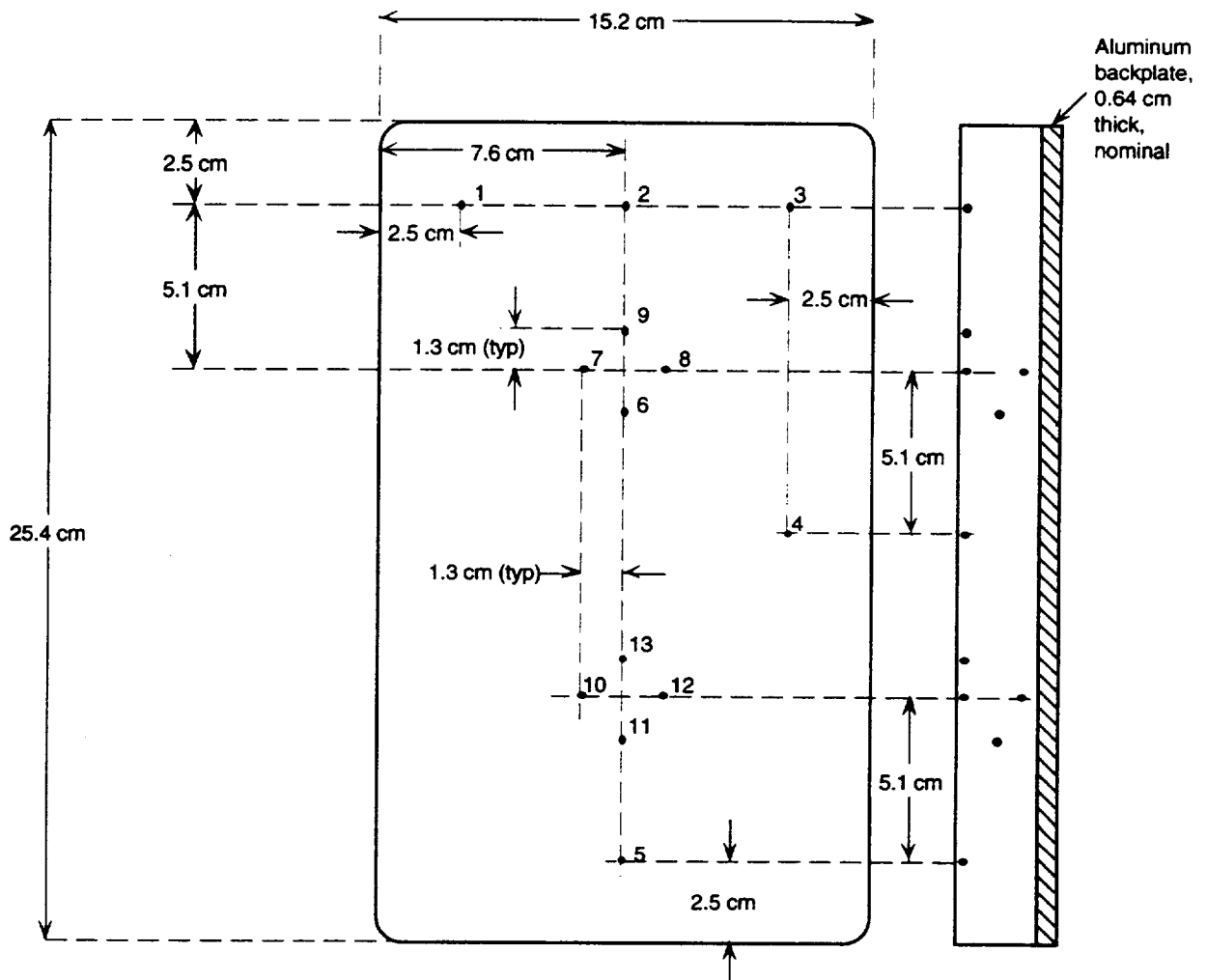
Figure A-1. Schematic of models SLAP01, SLAP02, SLAP03, and SLAP04.



Thermocouple depth
beneath surface

#	cm	#	cm
1	0.25	7	1.3
2	0.25	8	1.3
3	0.25	9	2.5
4	0.25	10	1.3
5	0.25	11	1.3
6	0.25	12	2.5

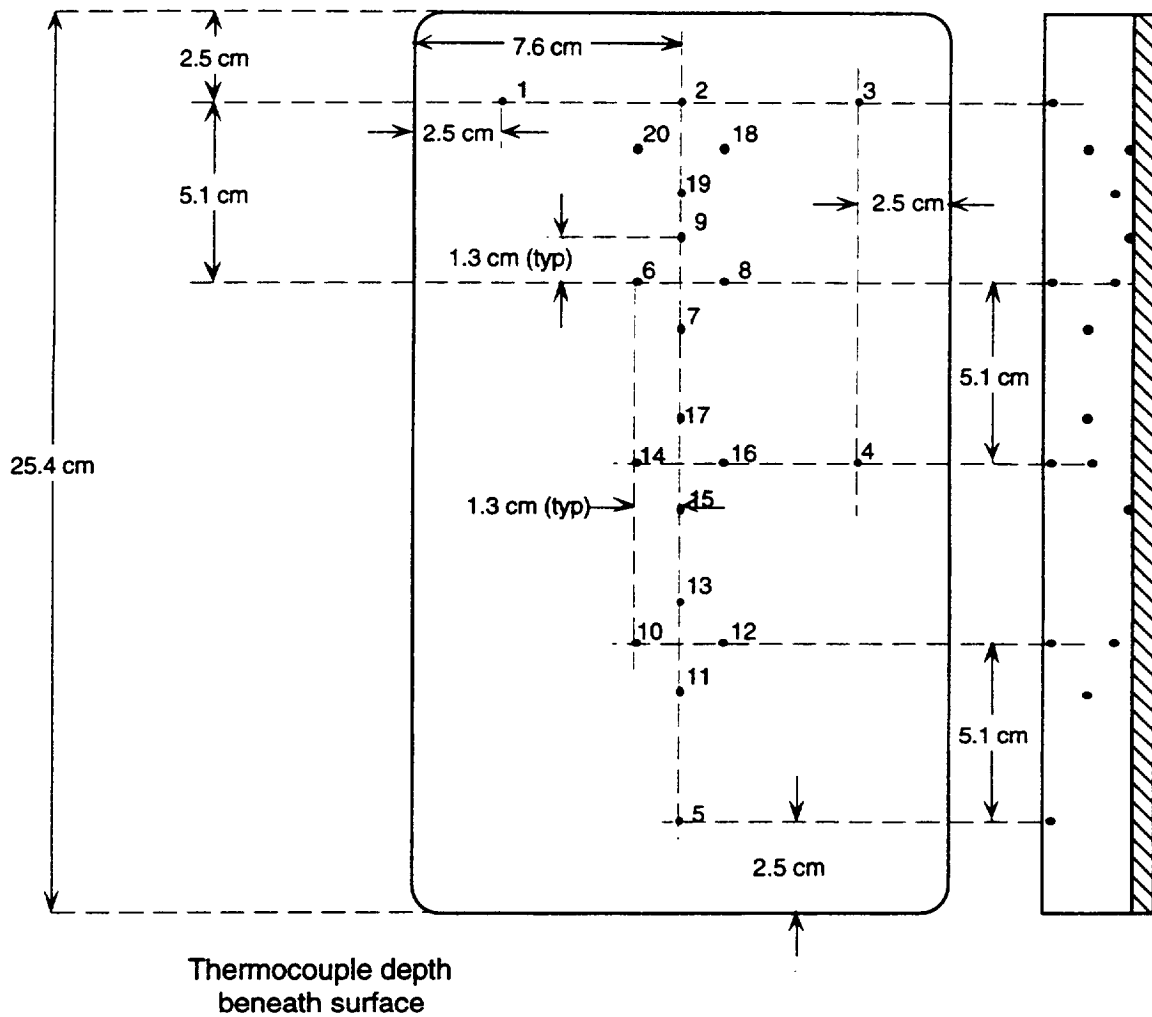
Figure A-2. Schematic of model SLAP05.



Thermocouple depth beneath surface

#	cm	#	cm
1	0.25	7	0.25
2	0.25	8	1.9
3	0.25	9	0.25
4	0.25	10	0.25
5	0.25	11	1.3
6	1.3	12	1.9
		13	0.25

Figure A-3. Schematic of model SLAP06.



#	cm	#	cm
1	0.25	11	1.3
2	0.25	12	1.9
3	0.25	13	2.5
4	0.25	14	0.25
5	0.25	15	2.5
6	0.25	16	1.9
7	1.3	17	1.3
8	1.9	18	1.3
9	0.25	19	1.9
10	0.25	20	2.5

Figure A-4. Schematic of model SLAP07.

Repairs on this panel are approximately 3.3 cm in diameter; approximately 3x3 honeycomb cells.

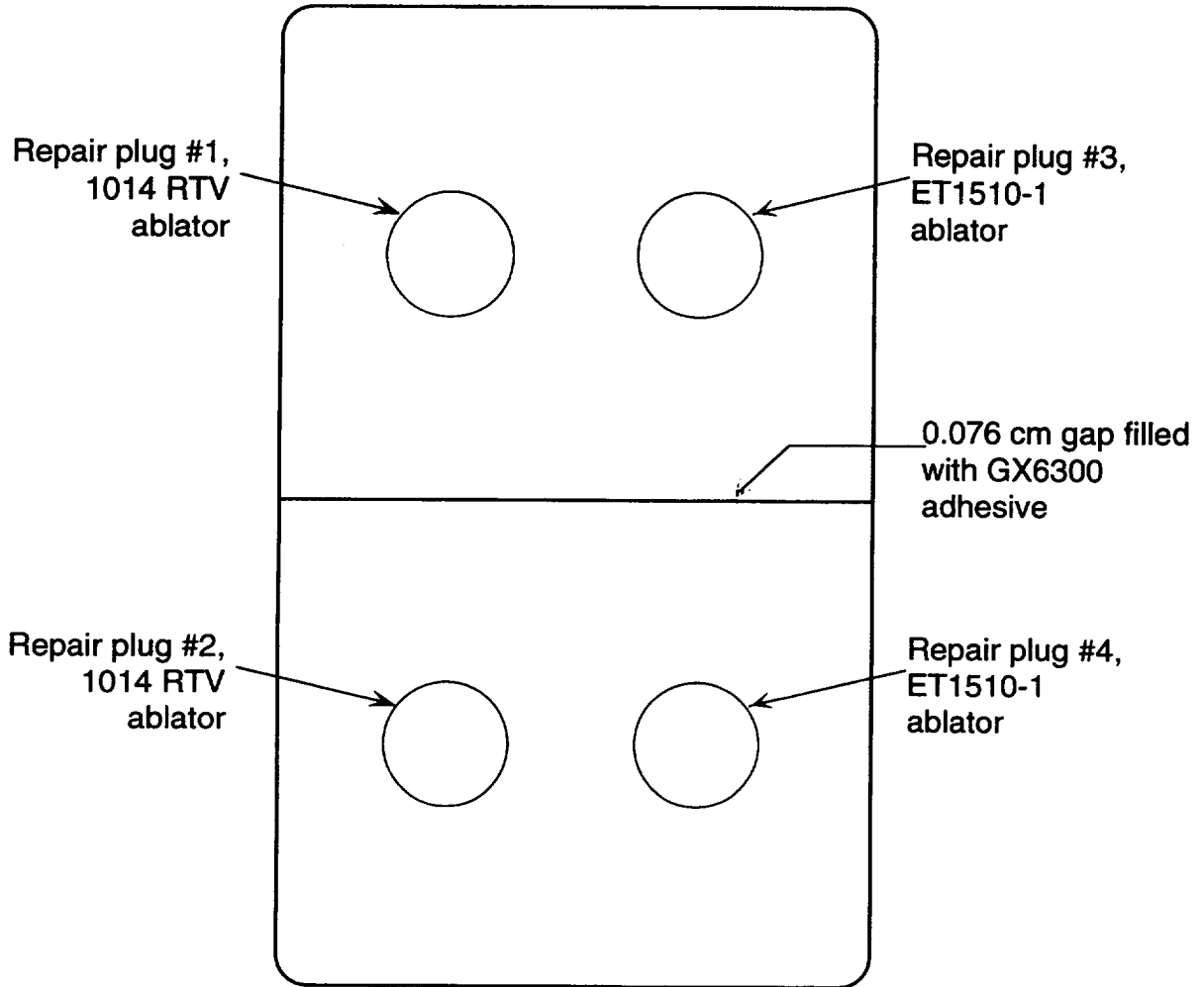


Figure A-5. Schematic of model SLAP08.

Repairs on this panel are approximately 1.5 cm in diameter; approximately 2x2 honeycomb cells.

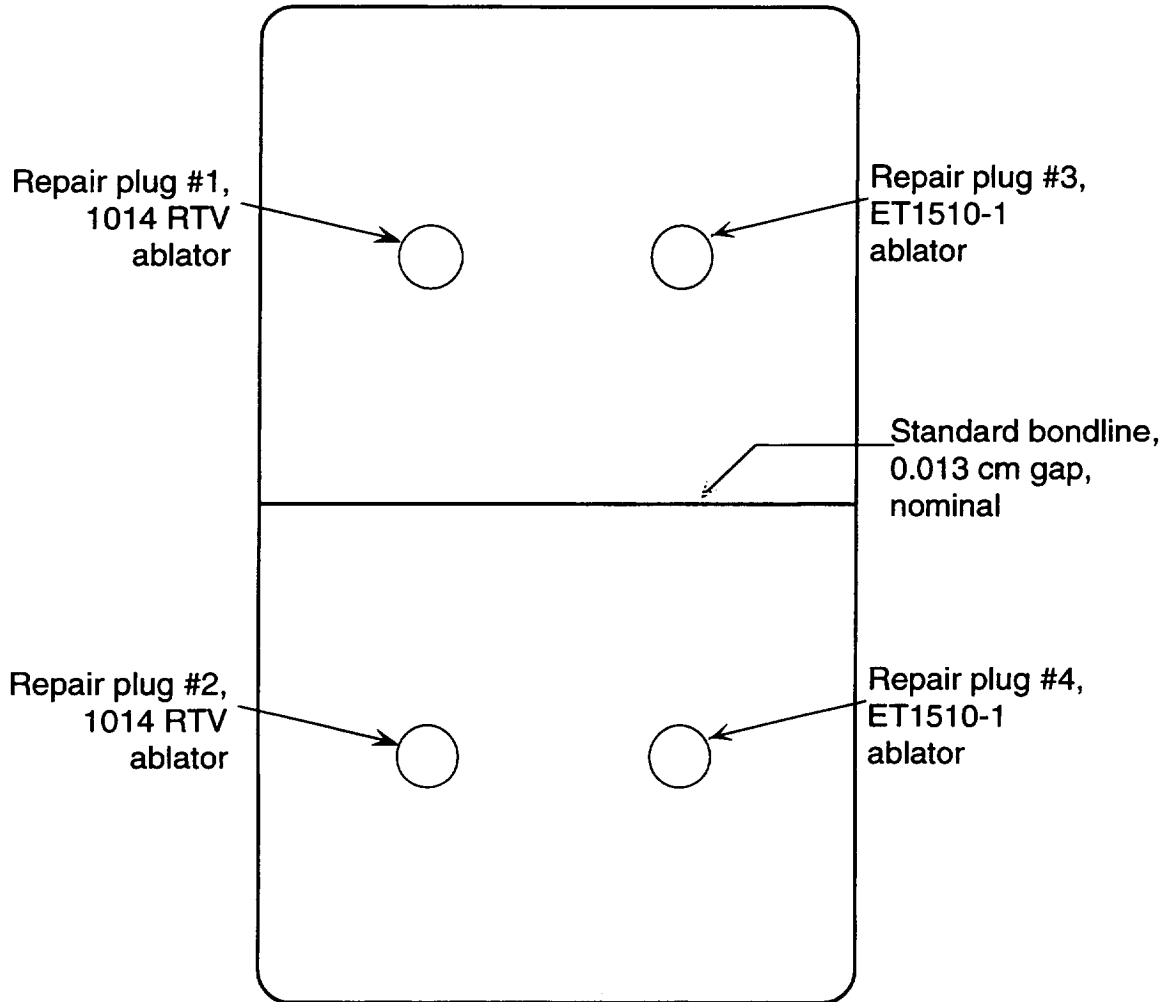


Figure A-6. Schematic of model SLAP09.

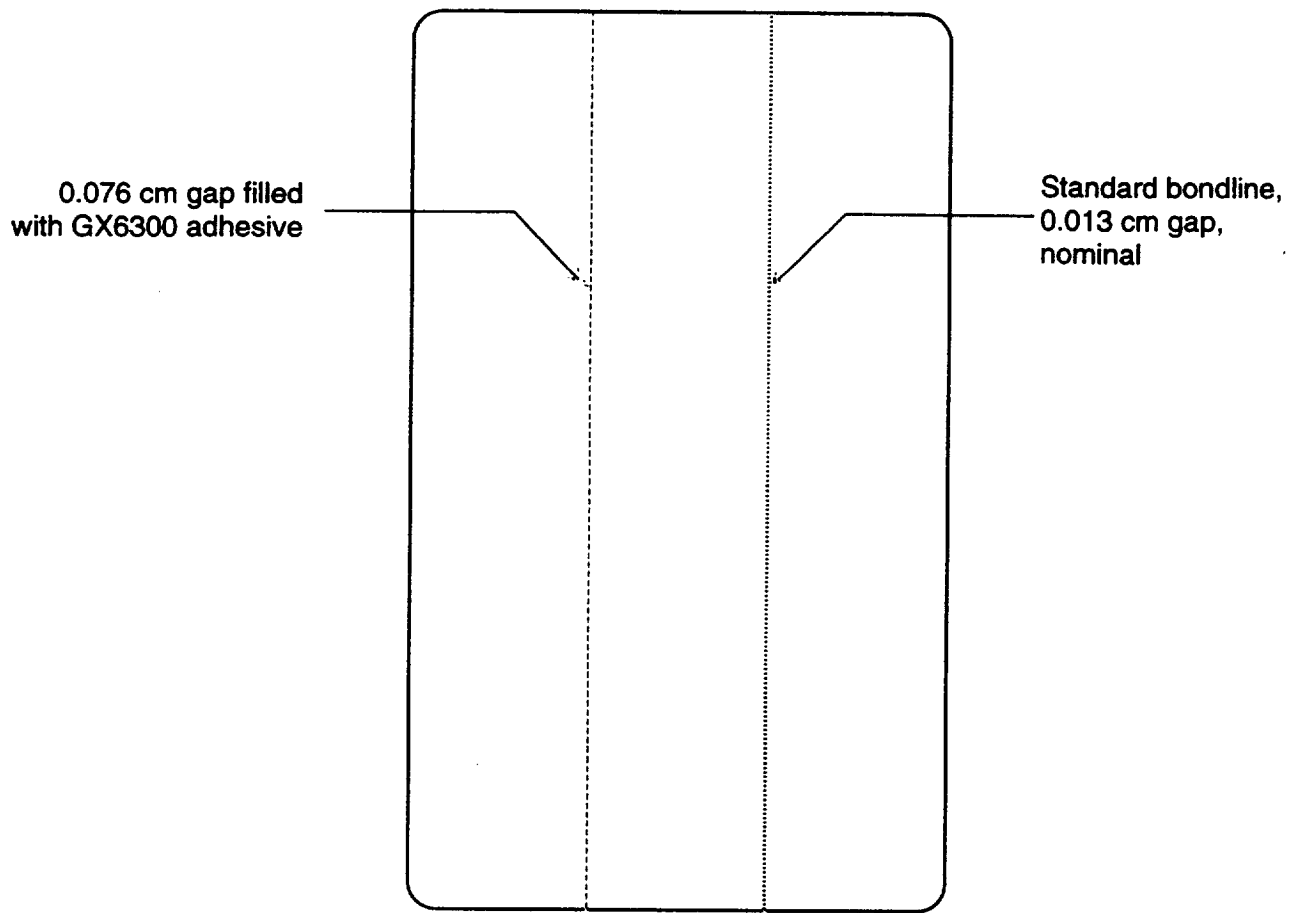


Figure A-7. Schematic of model SLAP10.

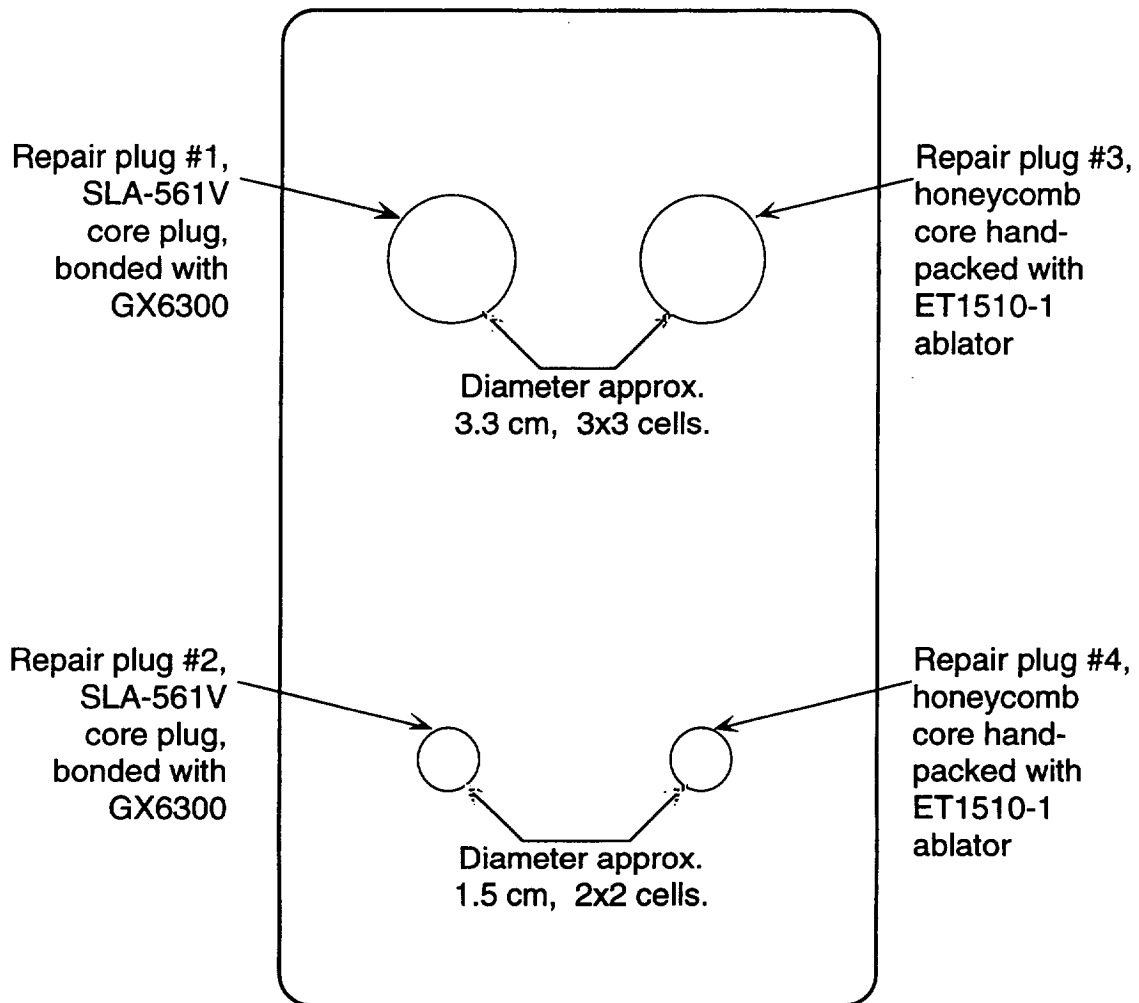
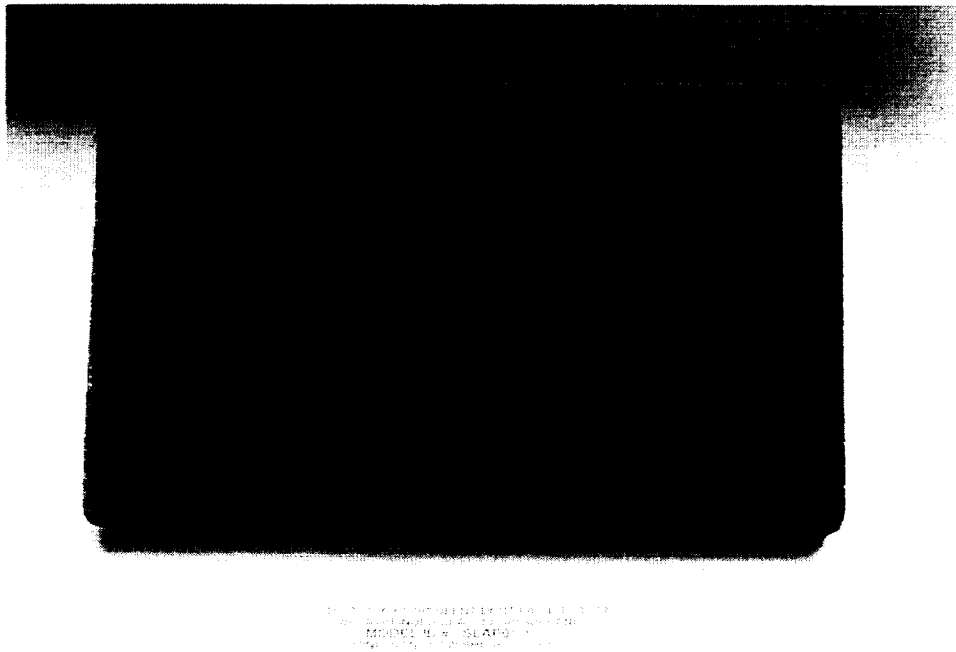


Figure A-8. Schematic of model SLAP11.

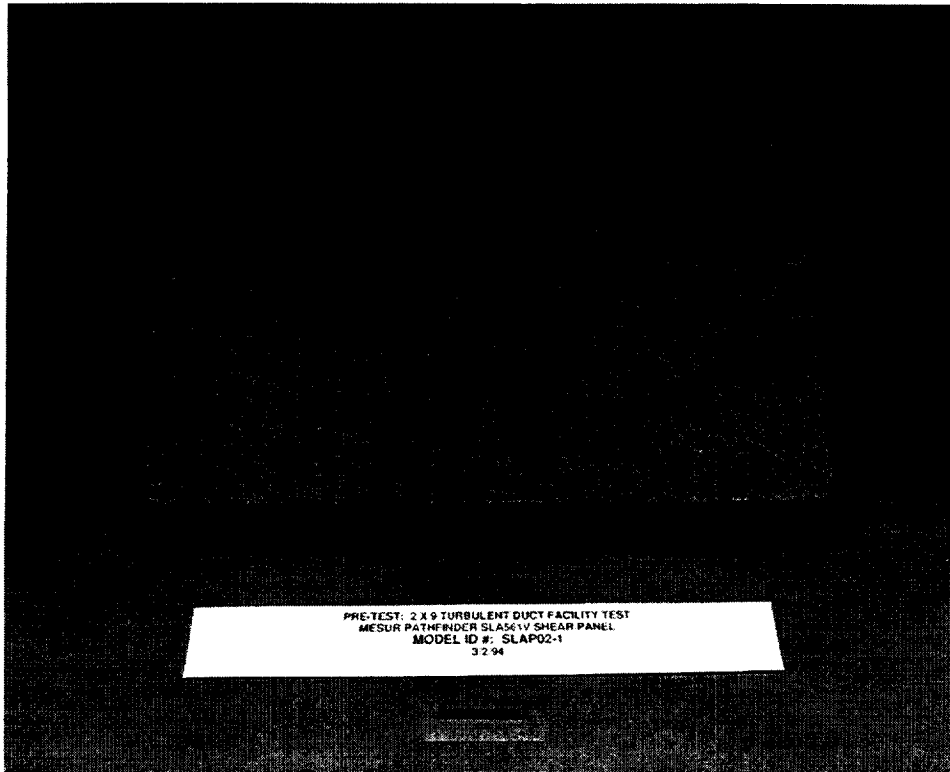


(a)

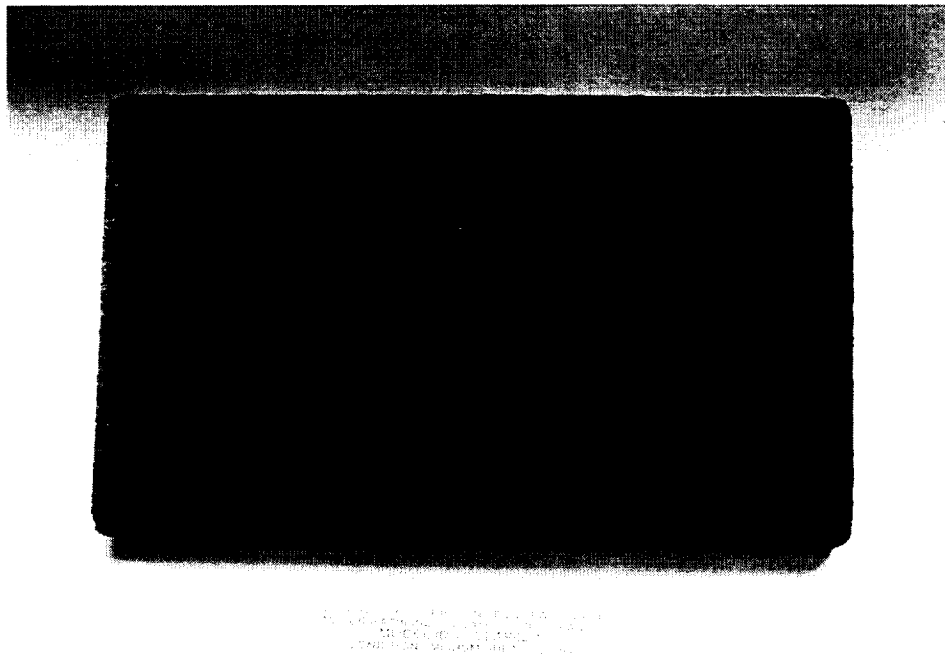


(b)

Figure A-9. Pre- and post-test photos of model SLAP01-1. (a) Ablation model SLAP01-1, (b) SLAP01-1 after 76 sec @ $\tau = 170 \text{ N/m}^2$, $\dot{q} = 21.6 \text{ W/cm}^2$.

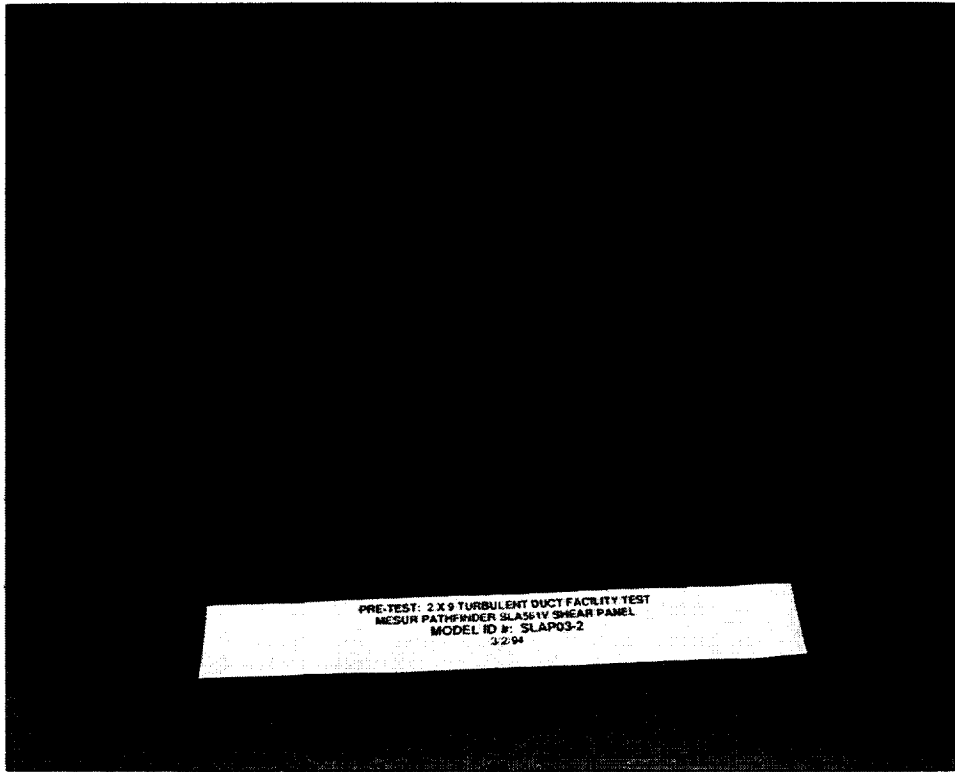


(a)

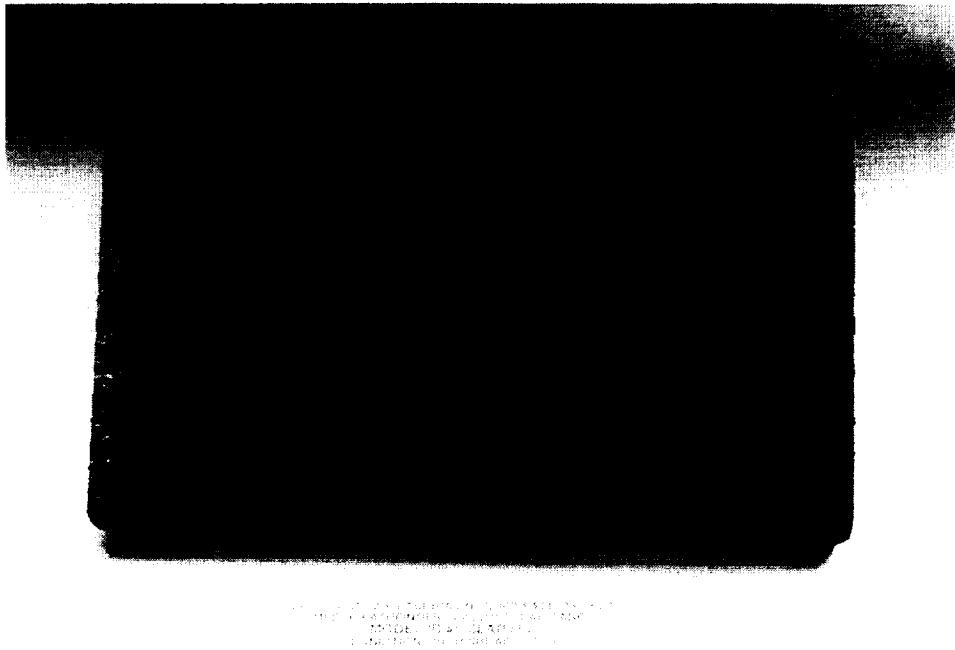


(b)

Figure A-10. Pre- and post-test photos of model SLAP02-2. (a) Ablation model SLAP02-2, (b) SLAP02-2 after 39 sec @ $\tau = 240 \text{ N/m}^2$, $\dot{q} = 40 \text{ W/cm}^2$.

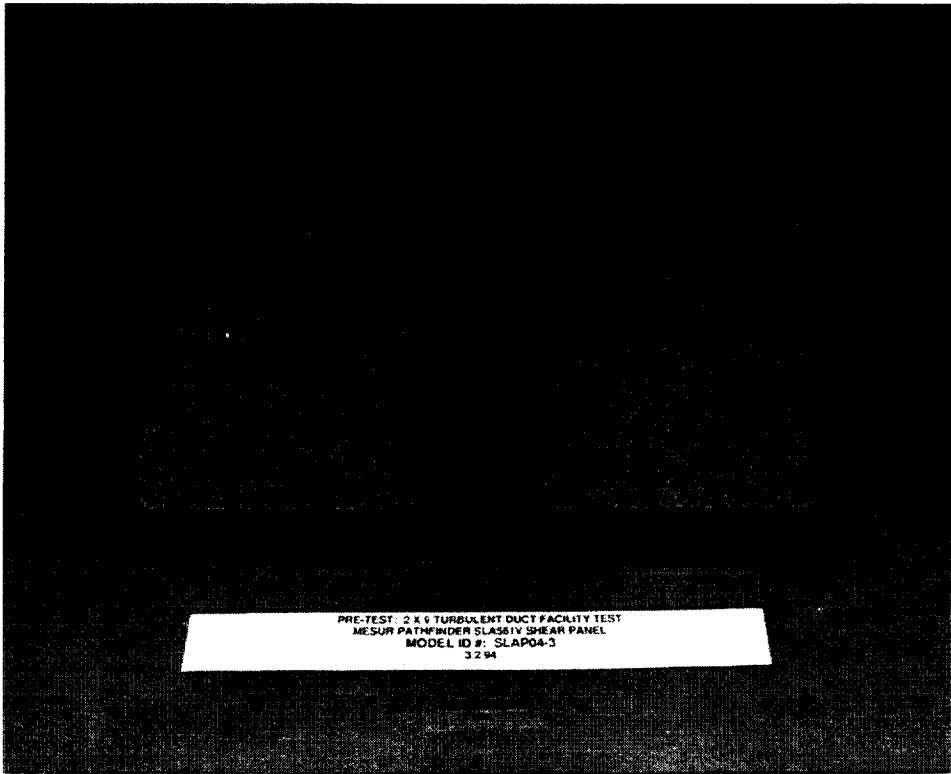


(a)

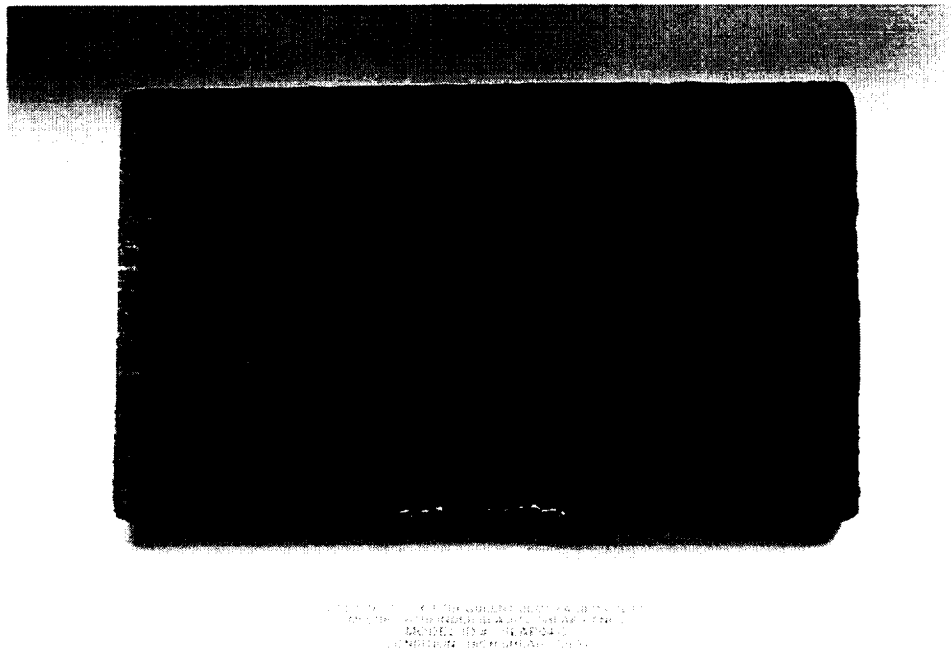


(b)

Figure A-11. Pre- and post-test photos of model SLAP03-3. (a) Ablation model SLAP03-3, (b) SLAP03-3 after 37 sec @ $\tau = 390 \text{ N/m}^2$, $\dot{q} = 51 \text{ W/cm}^2$.

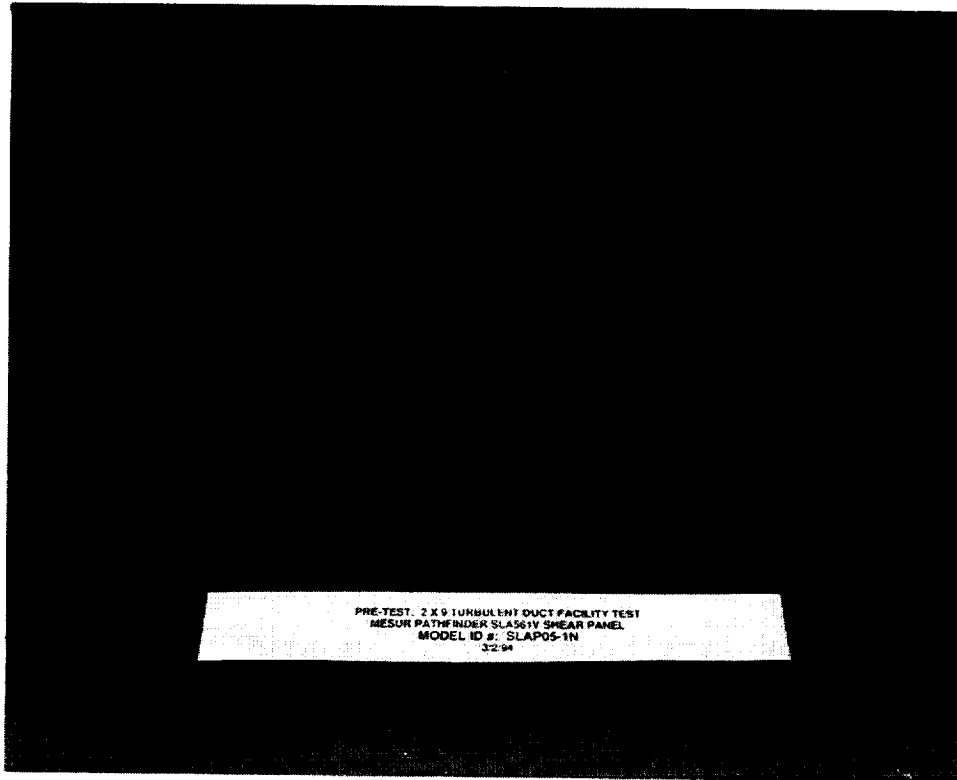


(a)

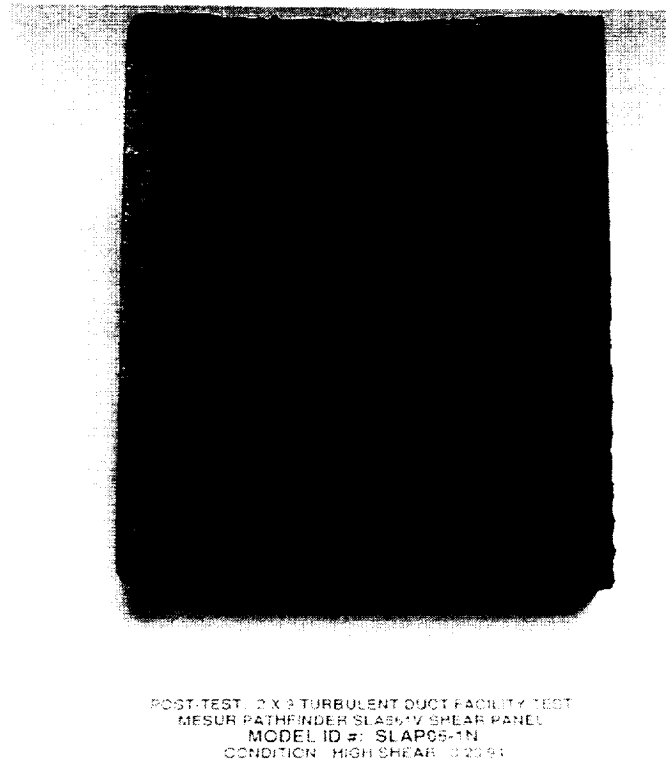


(b)

Figure A-12. Pre- and post-test photos of model SLAP04-3. (a) Ablation model SLAP04-3, (b) SLAP04-3 after 41 sec @ $\tau = 390 \text{ N/m}^2$, $\dot{q} = 51 \text{ W/cm}^2$.

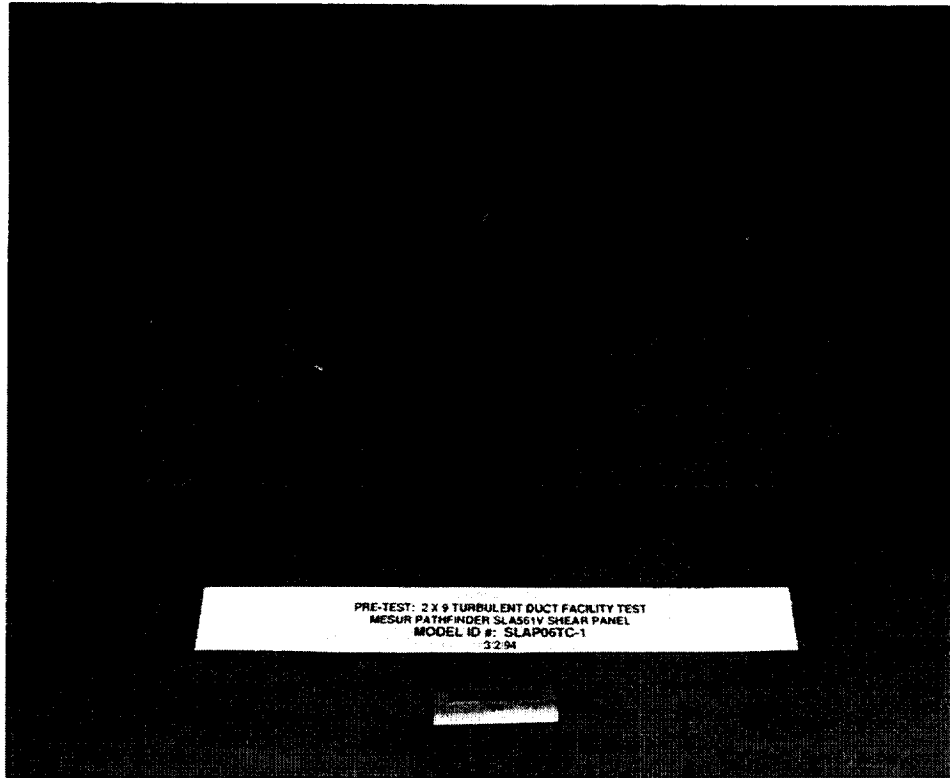


(a)

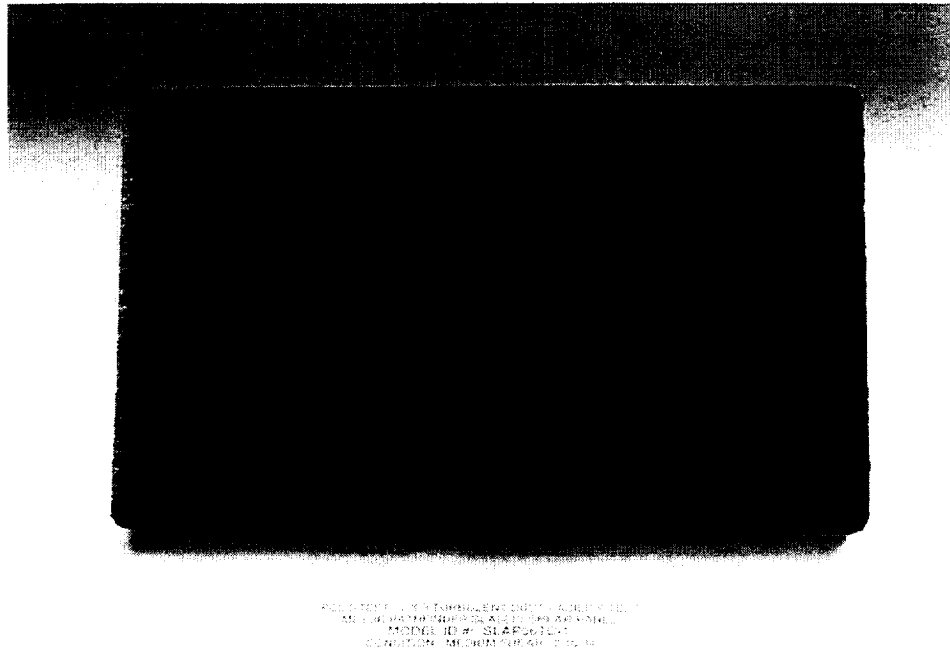


(b)

Figure A-13. Pre- and post-test photos of model SLAP05TC-3. (a) Instrumented model SLAP05TC-3, (b) SLAP05TC-3 after 31 sec @ $\tau = 390 \text{ N/m}^2$, $\dot{q} = 51 \text{ W/cm}^2$.



(a)

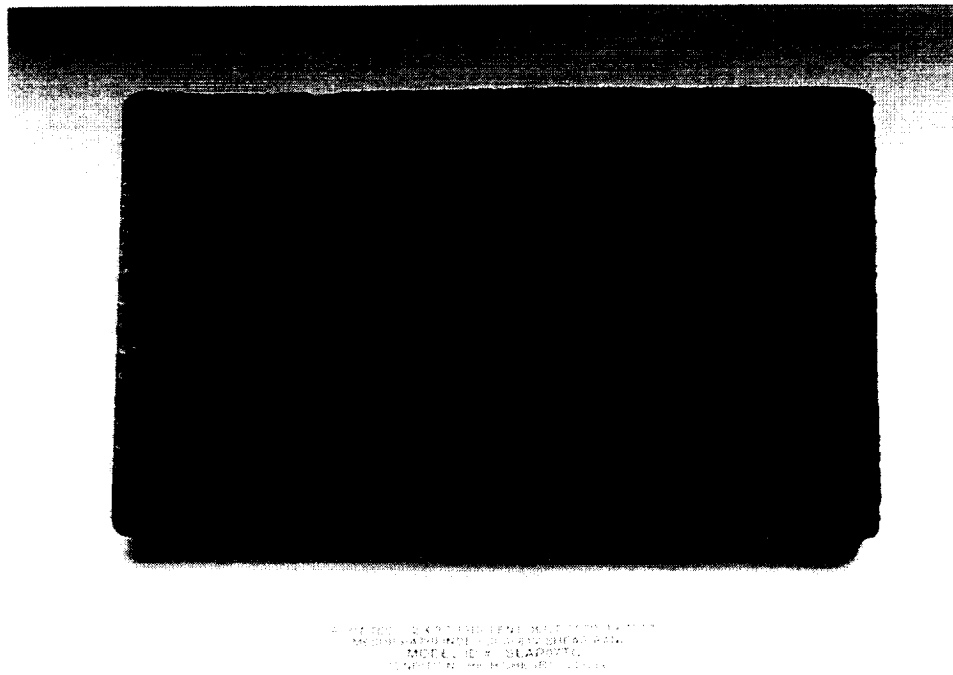


(b)

Figure A-14. Pre- and post-test photos of model SLAP06TC-2. (a) Instrumented model SLAP06TC-2, (b) SLAP06TC-2 after 38 sec @ $\tau = 240 \text{ N/m}^2$, $\dot{q} = 40 \text{ W/cm}^2$.

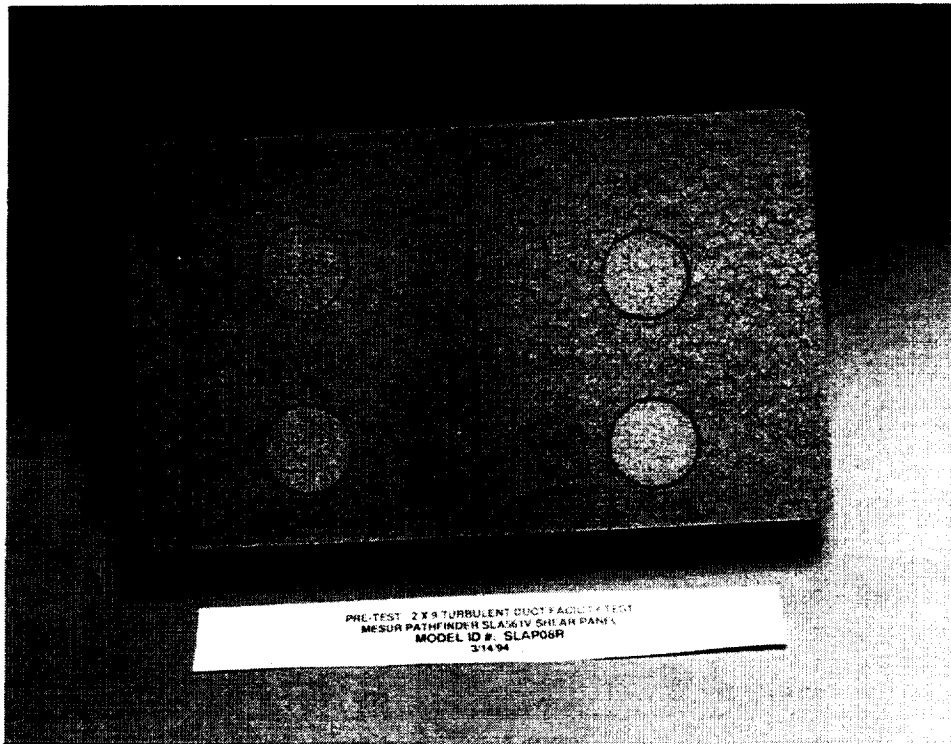


(a)

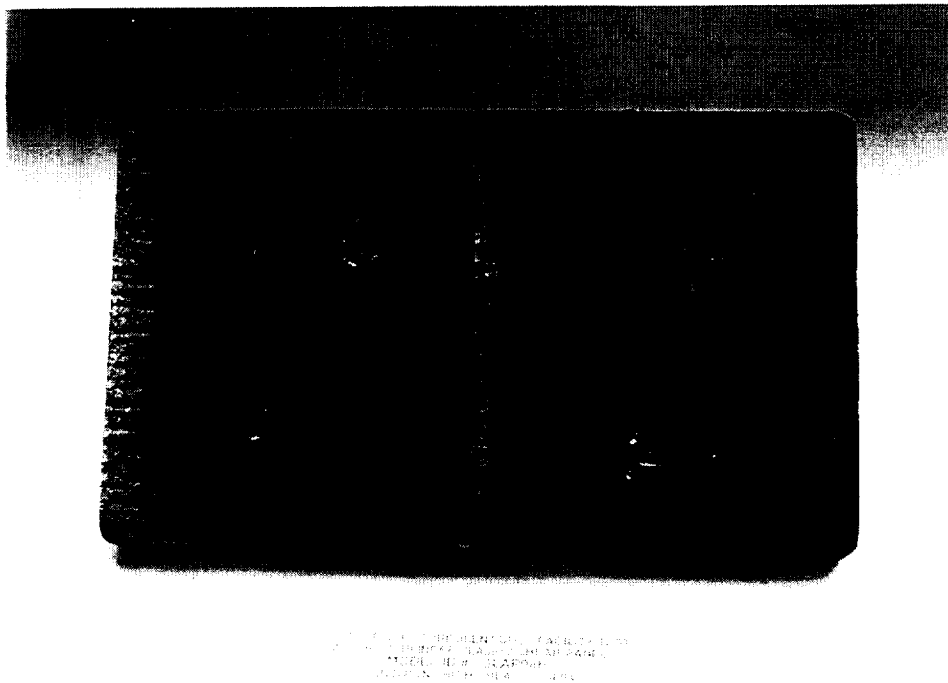


(b)

Figure A-15. Pre- and post-test photos of model SLAP07TC-3. (a) Instrumented model SLAP07TC-3, (b) SLAP07TC-3 after 48 sec @ $\tau = 390 \text{ N/m}^2$, $\dot{q} = 51 \text{ W/cm}^2$.

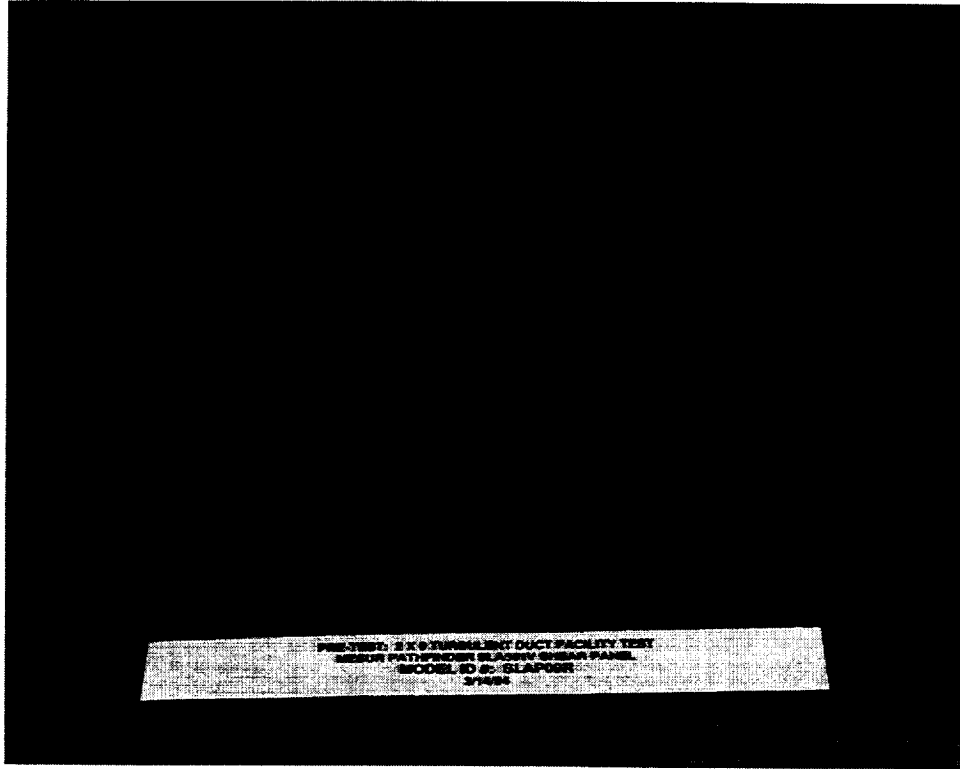


(a)

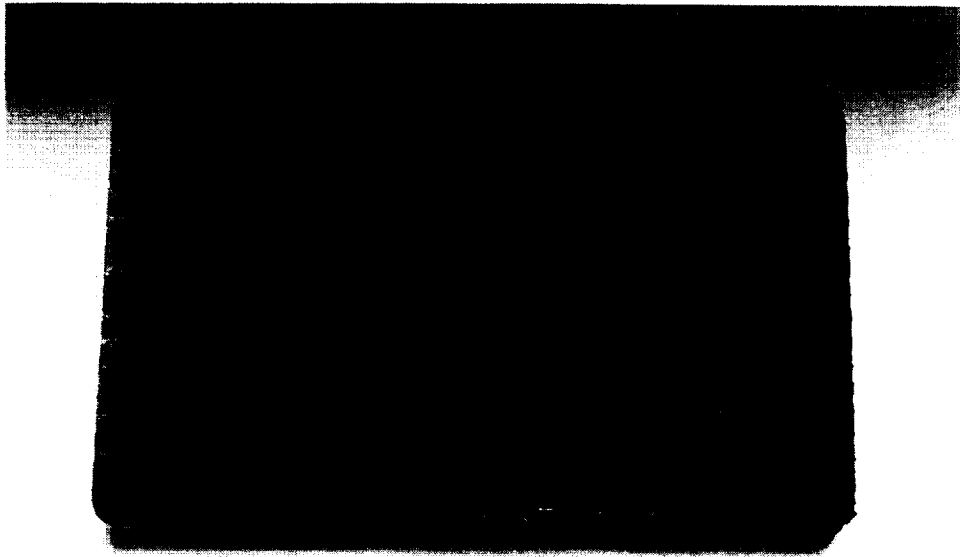


(b)

Figure A-16. Pre- and post-test photos of model SLAP08R-3. (a) Repair plug and gap model SLAP08R-3, (b) SLAP08R-3 after 38 sec @ $\tau = 390 \text{ N/m}^2$, $\dot{q} = 51 \text{ W/cm}^2$.

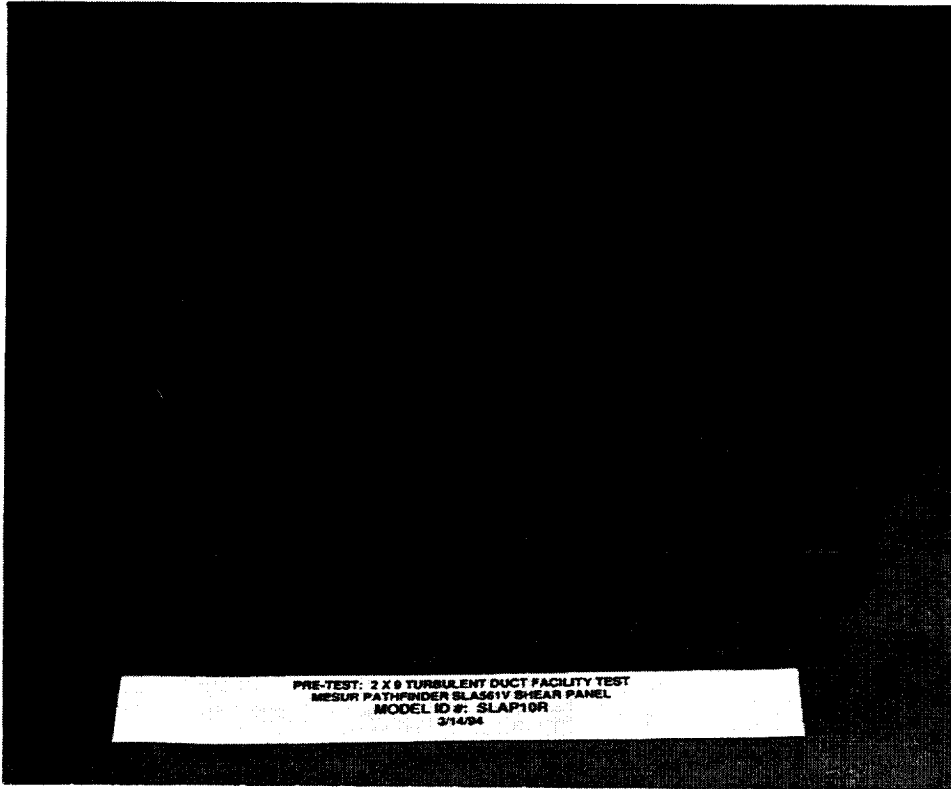


(a)

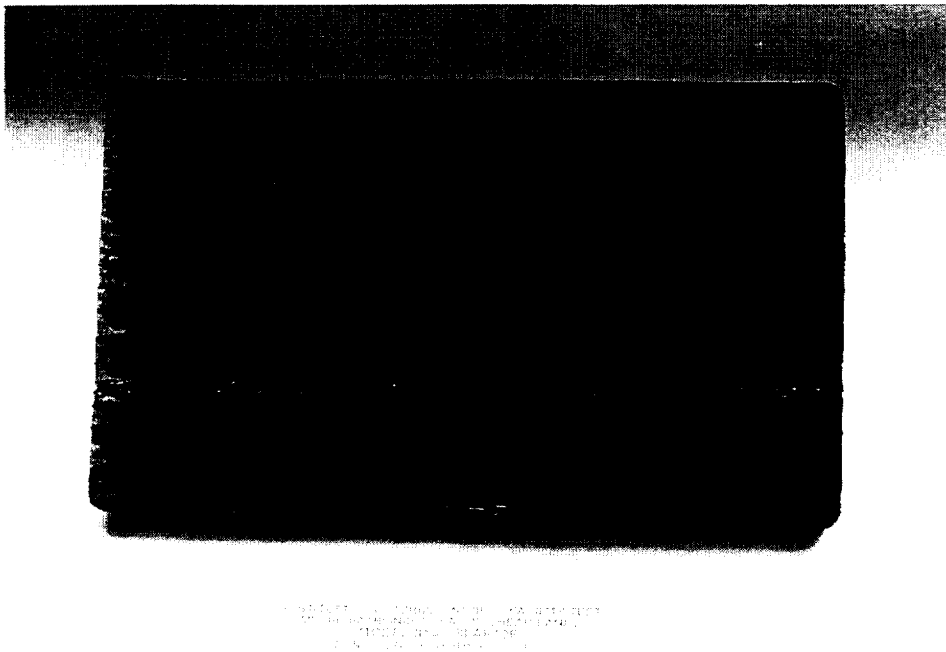


(b)

Figure A-17. Pre- and post-test photos of model SLAP09R-3. (a) Repair plug and gap model SLAP09R-3, (b) SLAP09R-3 after 40 sec @ $\tau = 390 \text{ N/m}^2$, $\dot{q} = 51 \text{ W/cm}^2$.

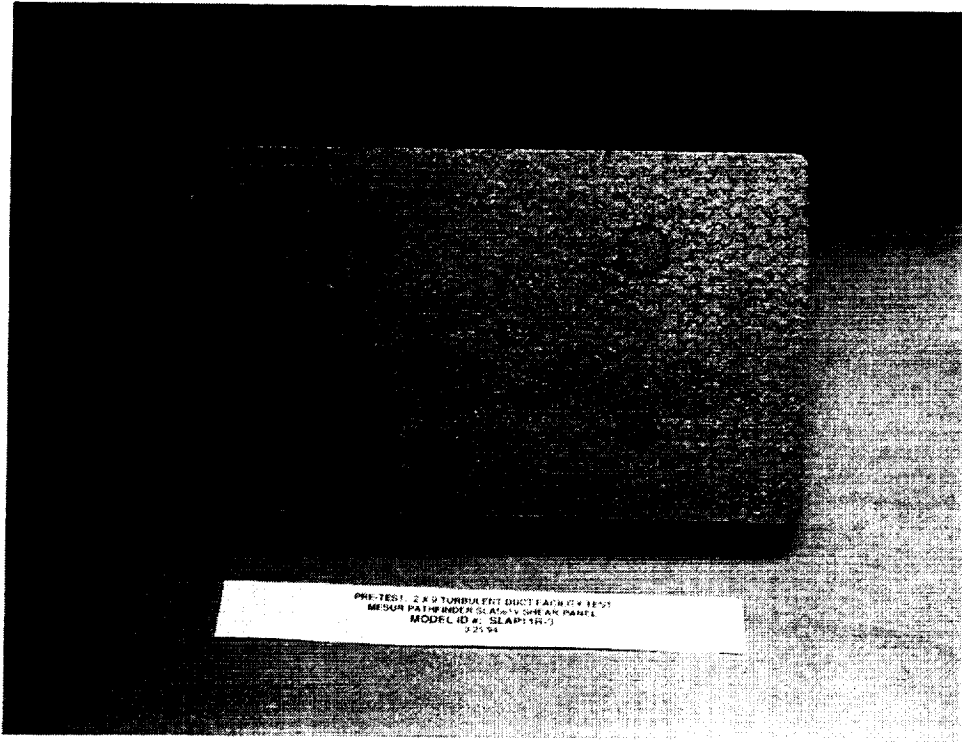


(a)

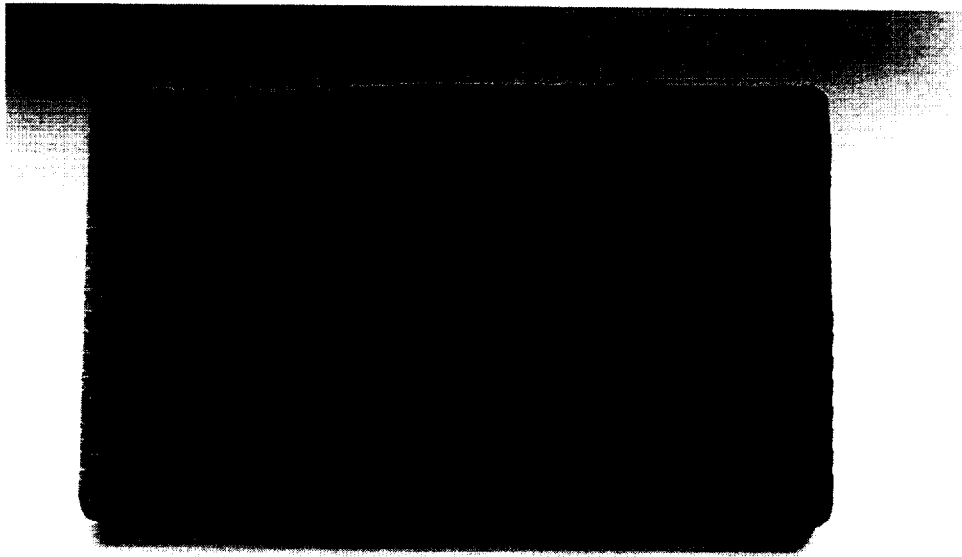


(b)

Figure A-18. Pre- and post-test photos of model SLAP10R-3. (a) Gap model SLAP10R-3, (b) SLAP10R-3 after 38 sec @ $\tau = 390 \text{ N/m}^2$, $\dot{q} = 51 \text{ W/cm}^2$.

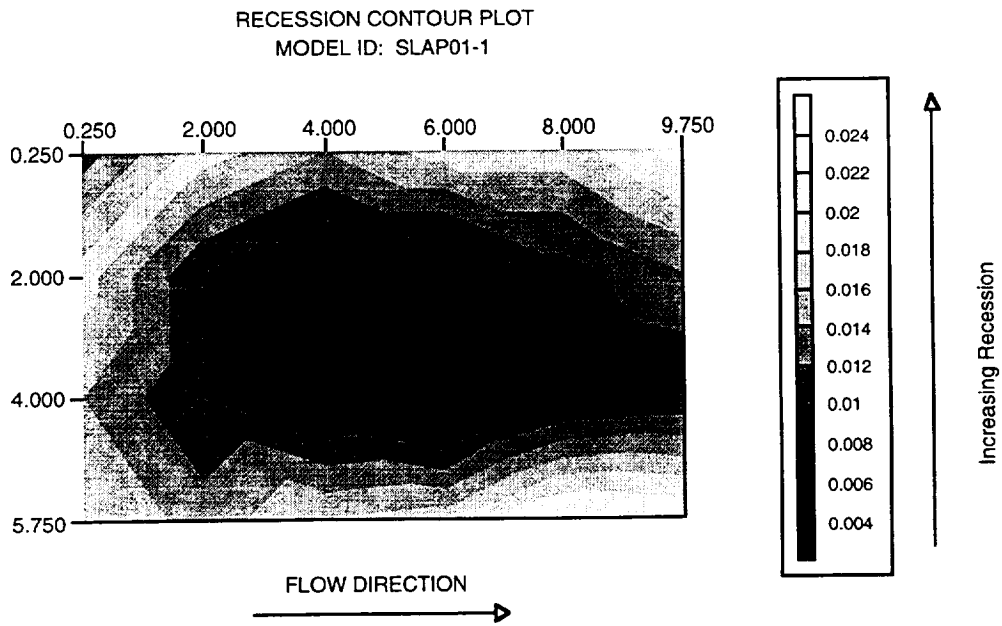


(a)



(b)

Figure A-19. Pre- and post-test photos of model SLAP11R-3. (a) Repair plug model SLAP11R-3, (b) SLAP11R-3 after 36 sec @ $\tau = 390 \text{ N/m}^2$, $\dot{q} = 51 \text{ W/cm}^2$.



Panel: 6 in. Width
10 in. Length
1 in. Height
Unit: Inches

Figure A-20. Recession contour plots of model SLAP01-1.

RECESSION CONTOUR PLOT
MODEL ID: SLAP02-2

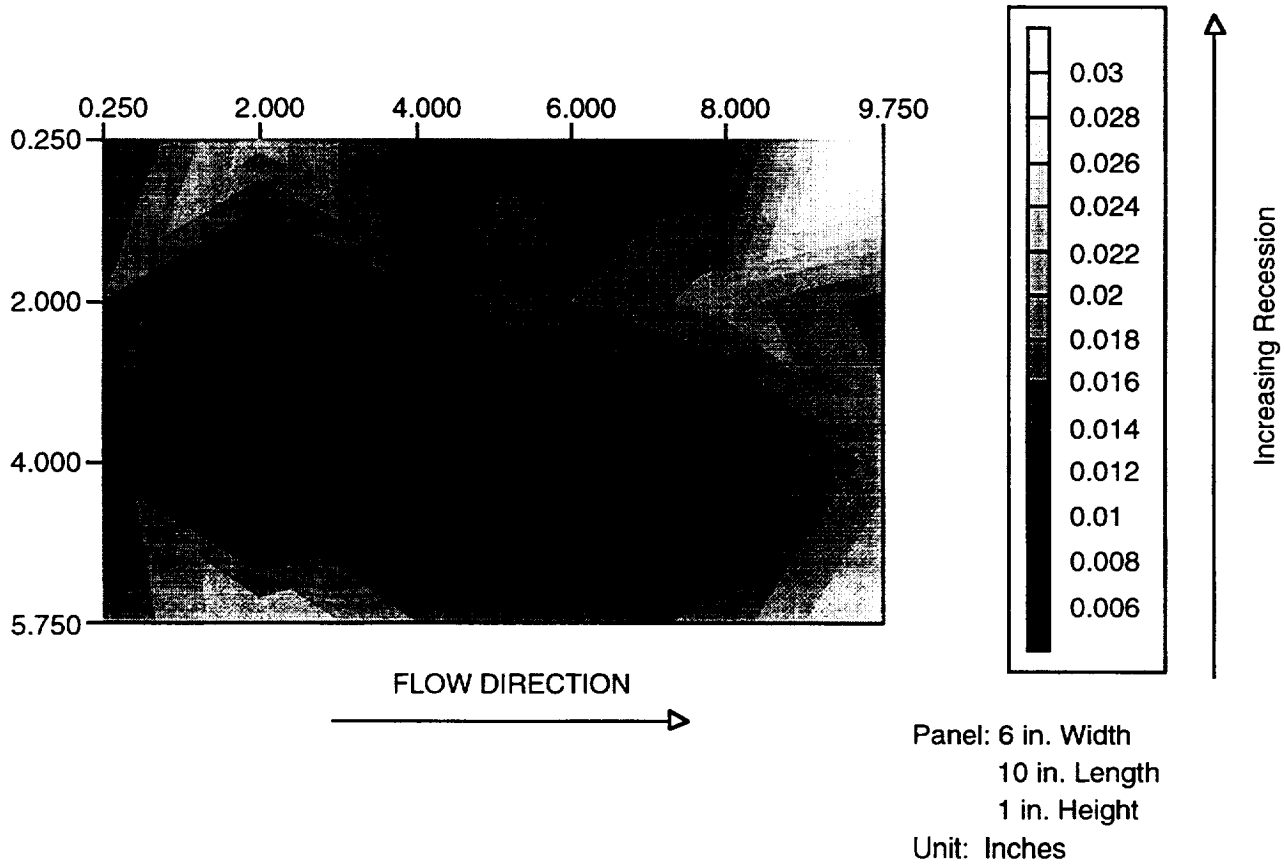
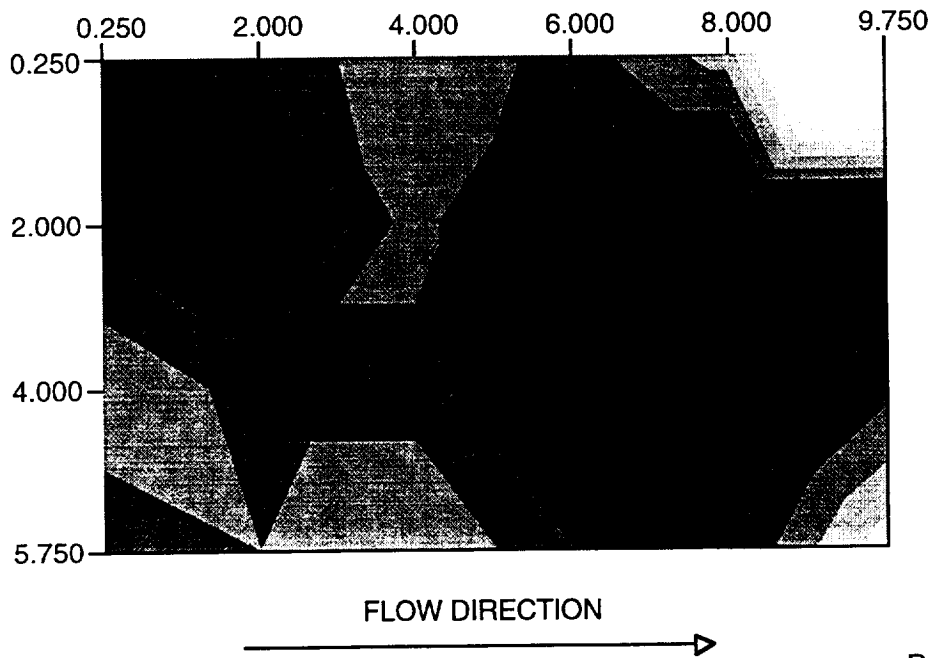


Figure A-21. Recession contour plots of model SLAP02-2.

RECESSION CONTOUR PLOT
MODEL ID: SLAP03-3



Panel: 6 in. Width
10 in. Length
1 in. Height
Unit: Inches

Figure A-22. Recession contour plots of model SLAP03-3.

RECESSION CONTOUR PLOT
MODEL ID: SLAP04-3

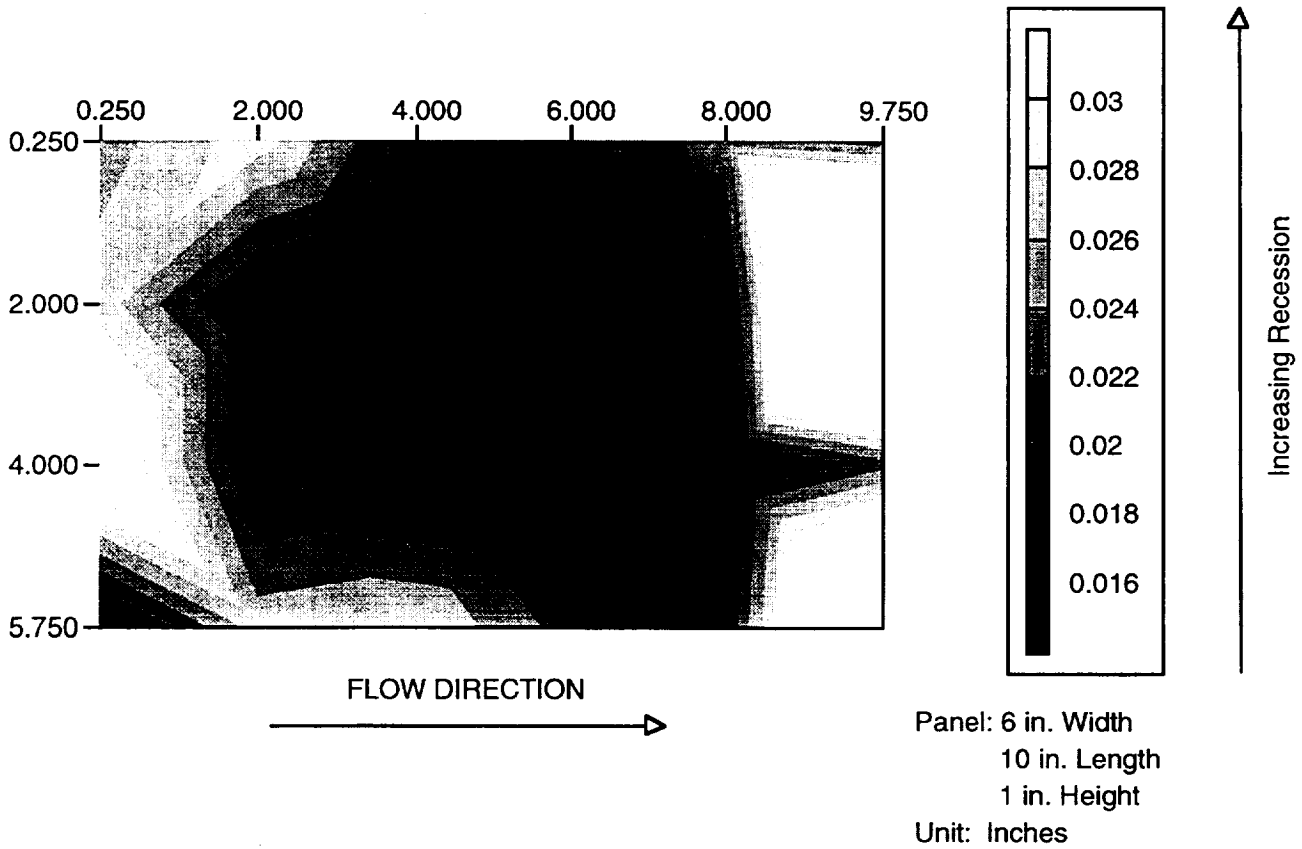
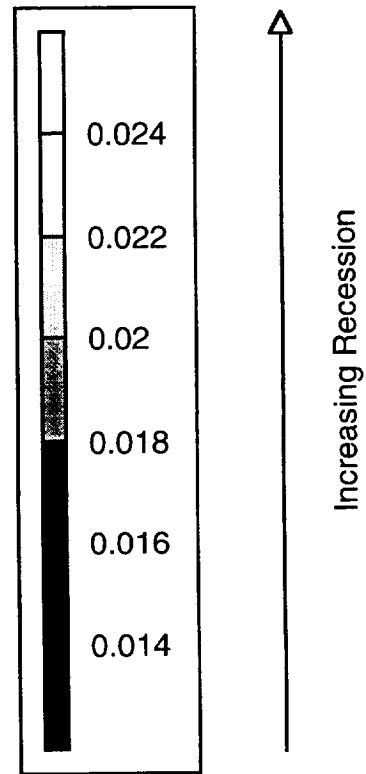
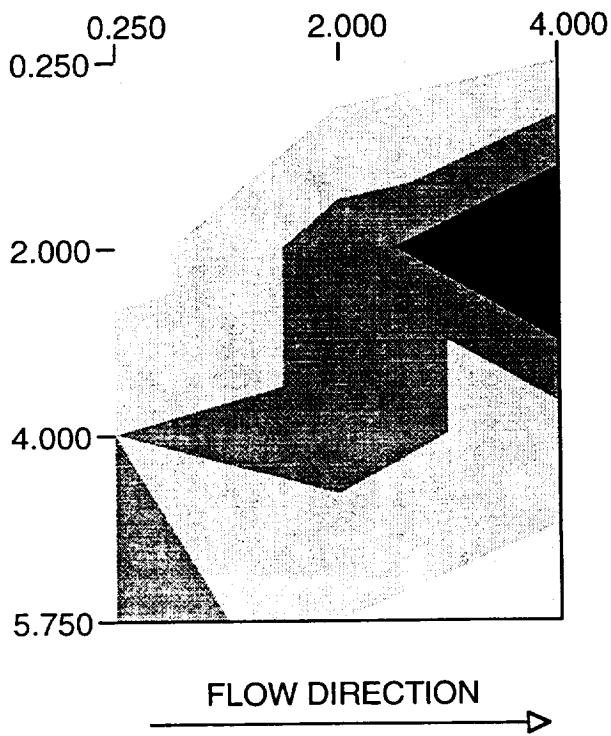


Figure A-23. Recession contour plots of model SLAP04-3.

RECESSION CONTOUR PLOT
MODEL ID: SLAP05TC-3



Panel: 6 in. Width
10 in. Length
1 in. Height
Unit: Inches

Figure A-24. Recession contour plots of model SLAP05TC-3.

RECESSION CONTOUR PLOT
MODEL ID: SLAP06TC-2

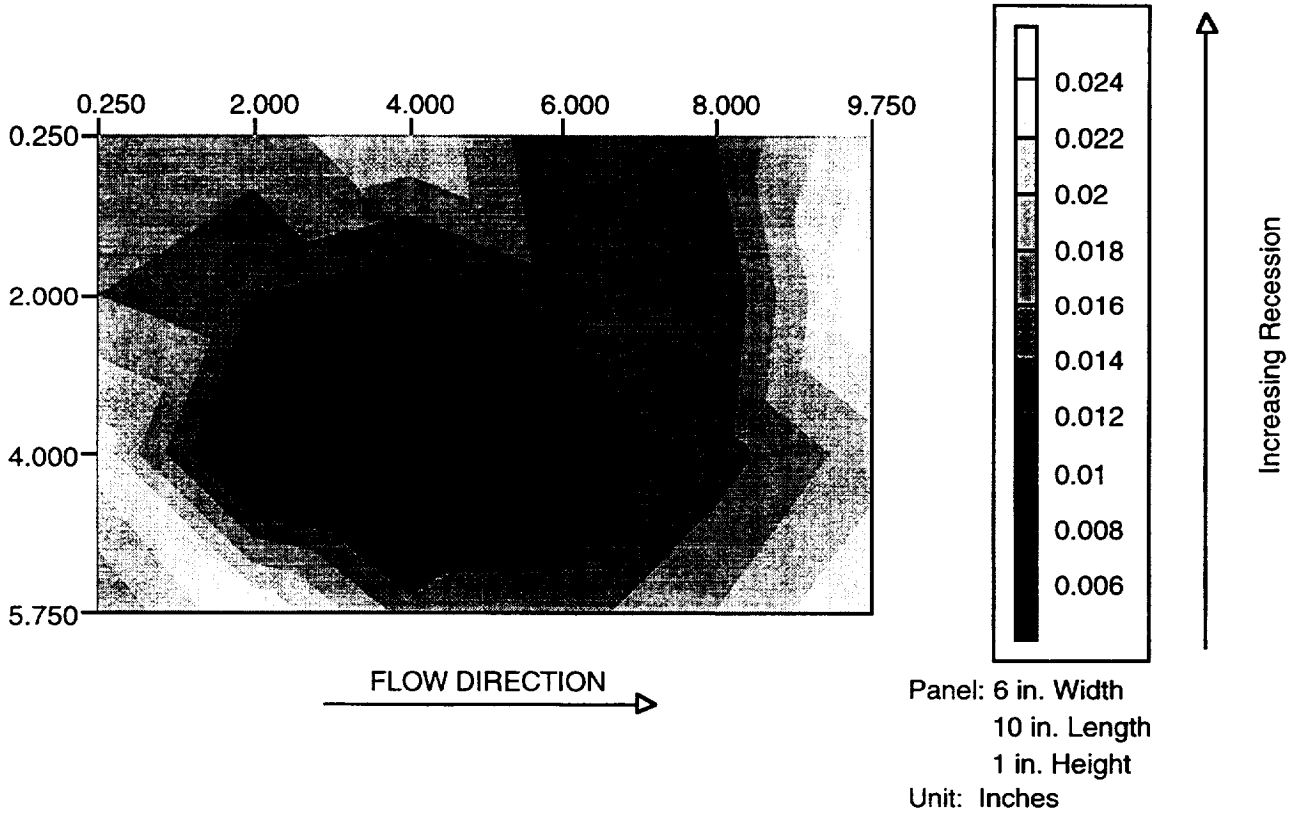
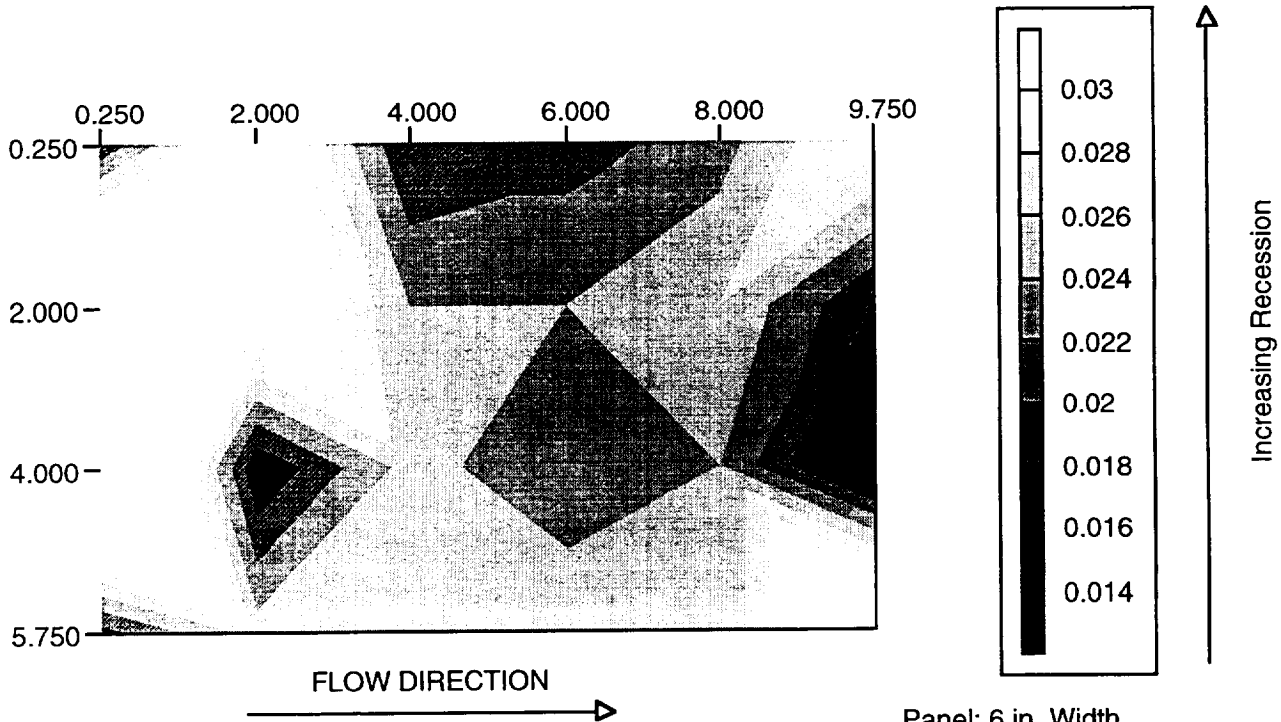


Figure A-25. Recession contour plots of model SLAP06TC-2.

RECESSION CONTOUR PLOT
MODEL ID: SLAP07TC-3



Panel: 6 in. Width
10 in. Length
1 in. Height
Unit: Inches

Figure A-26. Recession contour plots of model SLAP07TC-3.

RECESSION CONTOUR PLOT
MODEL ID: SLAP08R-3

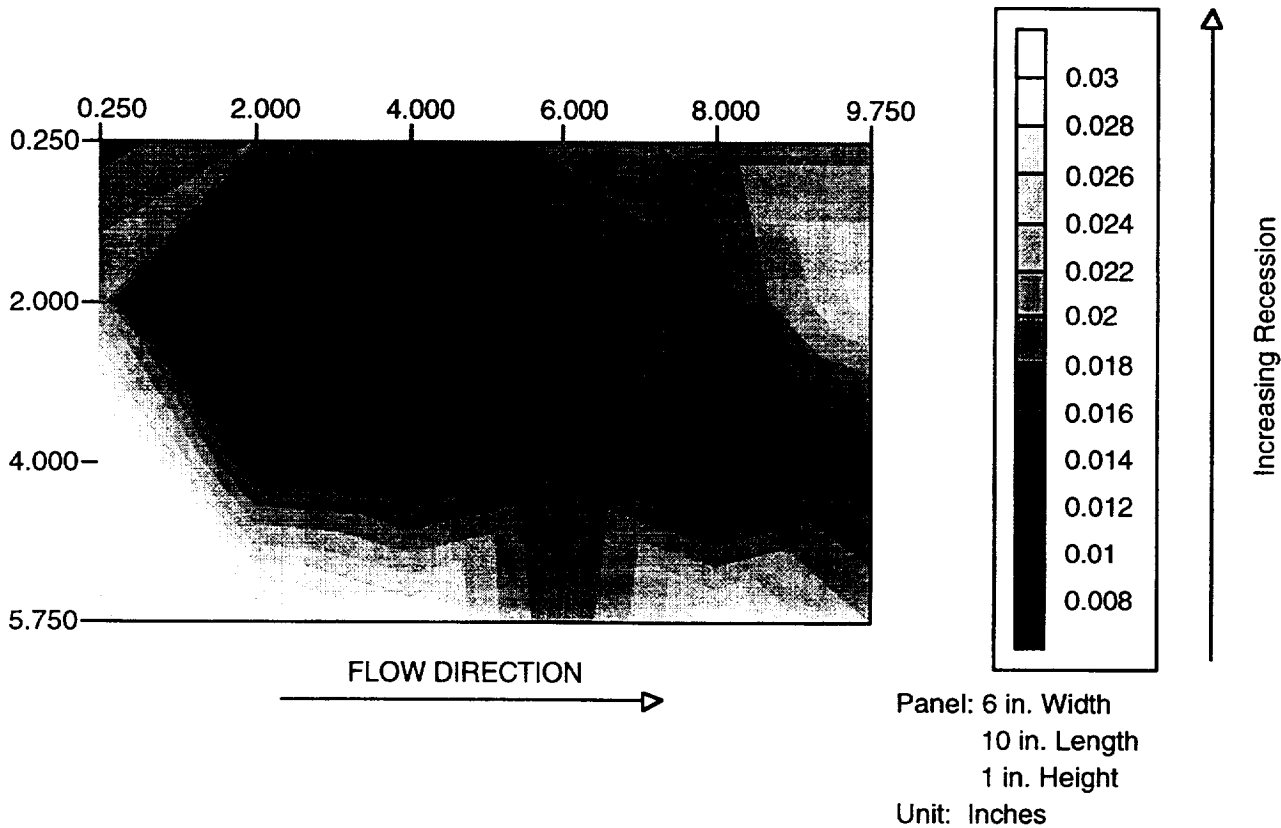


Figure A-27. Recession contour plots of model SLAP08R-3.

RECESSION CONTOUR PLOT/
MODEL ID: SLAP09R-3

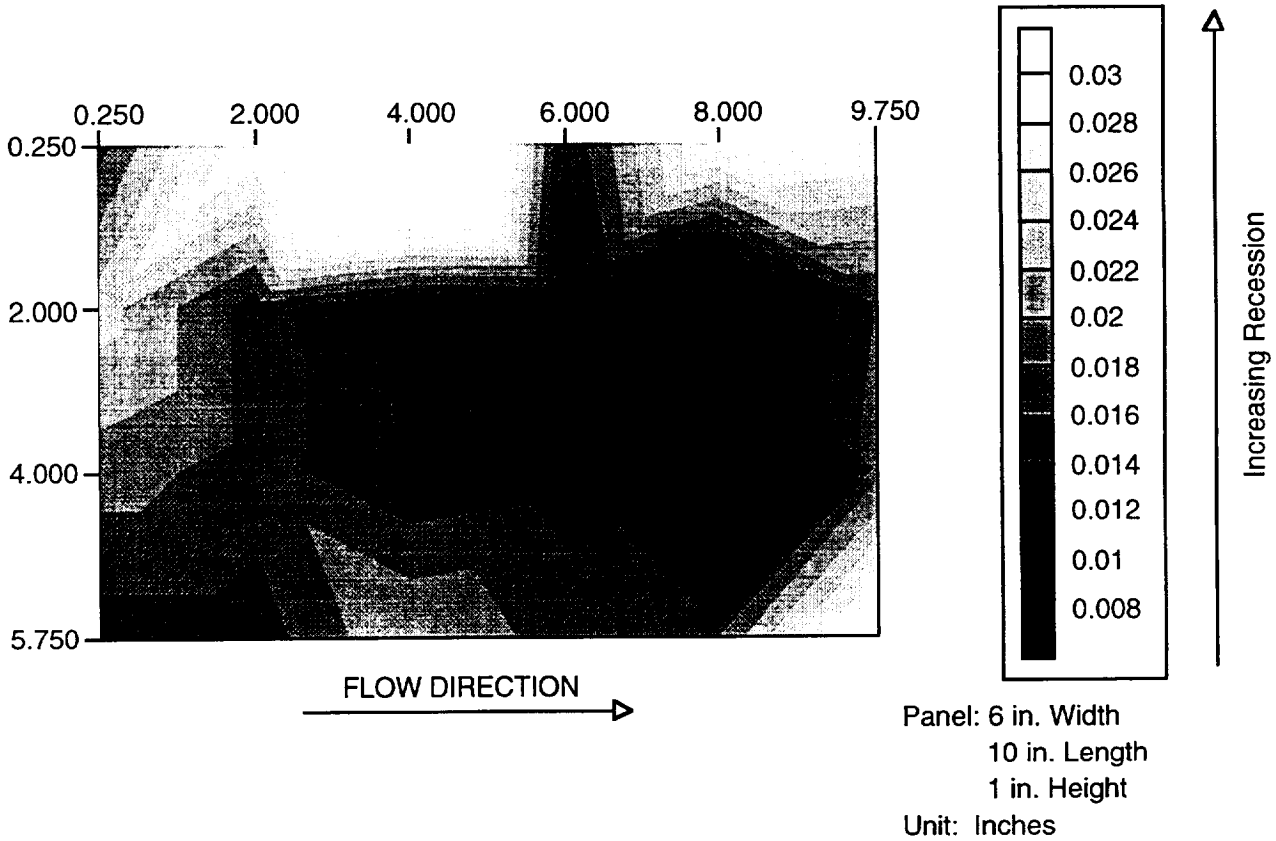


Figure A-28. Recession contour plots of model SLAP09R-3.

RECESSION CONTOUR PLOT
MODEL ID: SLAP010R-3

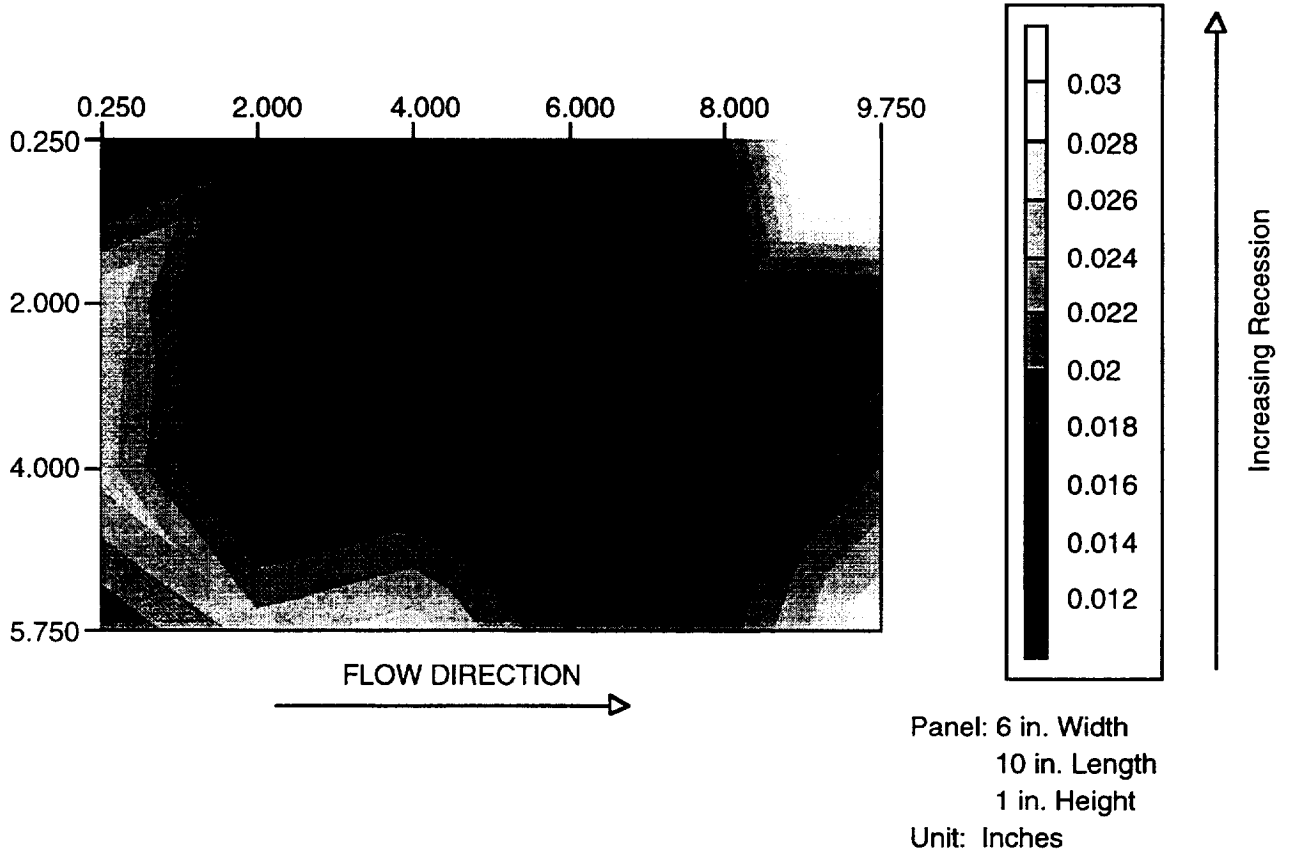


Figure A-29. Recession contour plots of model SLAP010R-3.

RECESSION CONTOUR PLOT
MODEL ID: SLAP011R-3

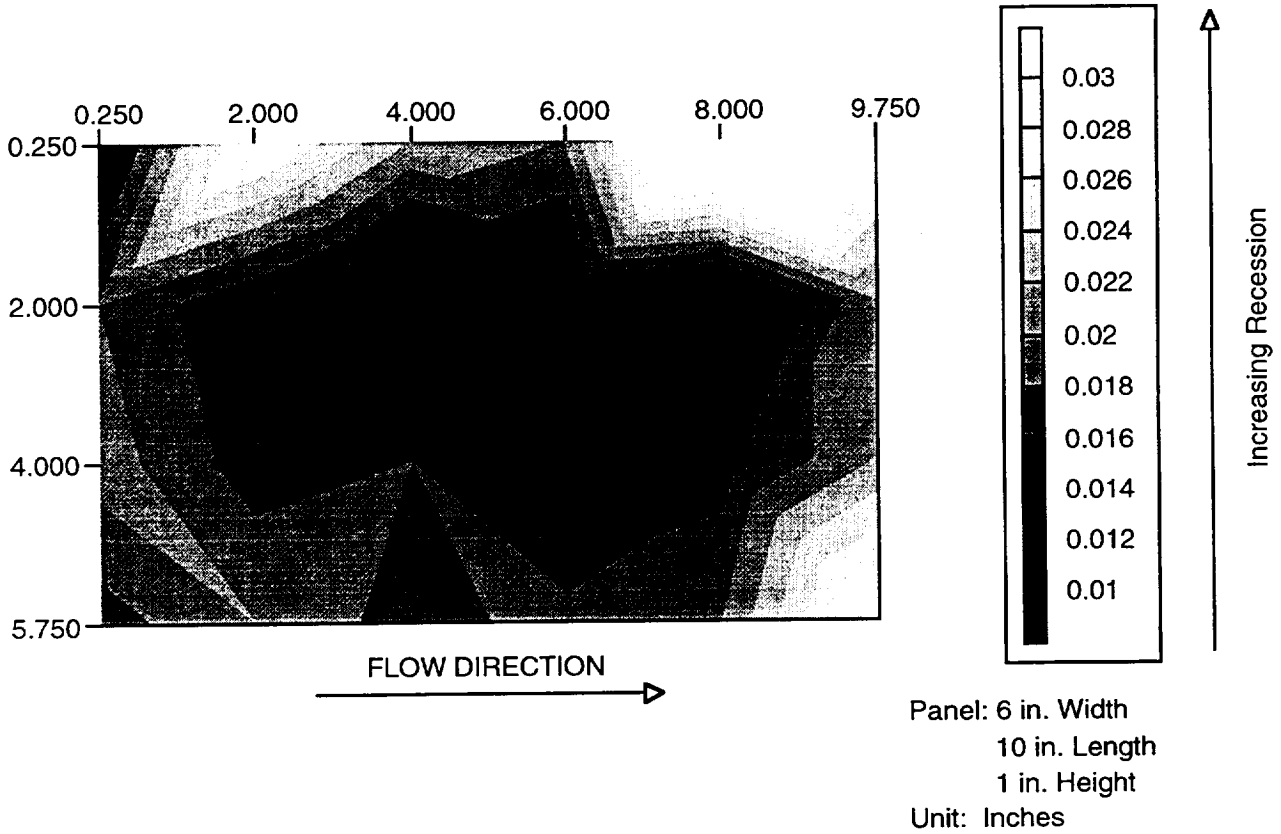


Figure A-30. Recession contour plots of model SLAP11R-3.

REPORT DOCUMENTATION PAGE

Form Approved
OMB No. 0704-0188

Public reporting burden for this collection of information is estimated to average 1 hour per response, including the time for reviewing instructions, searching existing data sources, gathering and maintaining the data needed, and completing and reviewing the collection of information. Send comments regarding this burden estimate or any other aspect of this collection of information, including suggestions for reducing this burden, to Washington Headquarters Services, Directorate for Information Operations and Reports, 1215 Jefferson Davis Highway, Suite 1204, Arlington, VA 22202-4302, and to the Office of Management and Budget, Paperwork Reduction Project (0704-0188), Washington, DC 20503.

1. AGENCY USE ONLY (Leave blank)	2. REPORT DATE September 1996	3. REPORT TYPE AND DATES COVERED Technical Memorandum	
4. TITLE AND SUBTITLE Ames Research Center Shear Tests of SLA-561V Heat Shield Material for Mars-Pathfinder		5. FUNDING NUMBERS 232-01-04	
6. AUTHOR(S) Huy Tran, Michael Tauber,* William Henline, Duoc Tran,* Alan Cartledge, Frank Hui, and Norm Zimmerman*		8. PERFORMING ORGANIZATION REPORT NUMBER A-961865	
7. PERFORMING ORGANIZATION NAME(S) AND ADDRESS(ES) Ames Research Center Moffett Field, CA 94035-1000		10. SPONSORING/MONITORING AGENCY REPORT NUMBER NASA TM-110402	
9. SPONSORING/MONITORING AGENCY NAME(S) AND ADDRESS(ES) National Aeronautics and Space Administration Washington, DC 20546-0001		11. SUPPLEMENTARY NOTES Point of Contact: Huy Tran, Ames Research Center, MS 234-1, Moffett Field, CA 94035-1000 (415) 604-0219 *Thermosciences Institute, Moffett Field, California	
12a. DISTRIBUTION/AVAILABILITY STATEMENT Unclassified-Unlimited Subject Category - 05		12b. DISTRIBUTION CODE	
13. ABSTRACT (Maximum 200 words) This report describes the results of arc-jet testing at Ames Research Center on behalf of Jet Propulsion Laboratory (JPL) for the development of the Mars-Pathfinder heat shield. The current test series evaluated the performance of the ablating SLA-561V heat shield material under shear conditions. In addition, the effectiveness of several methods of repairing damage to the heat shield were evaluated. A total of 26 tests were performed in March 1994 in the 2" x 9" arc-heated Turbulent Duct Facility, including runs to calibrate the facility to obtain the desired shear stress conditions. A total of eleven models were tested. Three different conditions of shear and heating were used. The non-ablating surface shear stresses and the corresponding, approximate, non-ablating surface heating rates were as follows: Condition I, 170 N/m ² and 22 W/cm ² ; Condition II, 240 N/m ² and 40 W/cm ² ; Condition III, 390 N/m ² and 51 W/cm ² . The peak shear stress encountered in flight is represented approximately by Condition I; however, the heating rate was much less than the peak flight value. The peak heating rate that was available in the facility (at Condition III) was about 30 percent less than the maximum value encountered during flight. Seven standard ablation models were tested, of which three models were instrumented with thermocouples to obtain in-depth temperature profiles and temperature contours. An additional four models contained a variety of repair plugs, gaps, and seams. These models were used to evaluate different repair materials and techniques, and the effect of gaps and construction seams. Mass loss and surface recession measurements were made on all models. The models were visually inspected and photographed before and after each test. The SLA-561V performed well; even at test Condition III, the char remained intact. Most of the resins used for repairs and gap fillers performed poorly. However, repair plugs made of SLA-561V performed well. Approximately 70 percent of the thermocouples yielded good data.			
14. SUBJECT TERMS Planetary exploration, Thermal protection system, Space vehicle		15. NUMBER OF PAGES 49	
		16. PRICE CODE A03	
17. SECURITY CLASSIFICATION OF REPORT Unclassified	18. SECURITY CLASSIFICATION OF THIS PAGE Unclassified	19. SECURITY CLASSIFICATION OF ABSTRACT	20. LIMITATION OF ABSTRACT